UNIVERSITY OF GOTHENBURG

DEPARTMENT OF EARTH SCIENCES

Change Analysis of the Stenungsund Landslide Using UAV and Airborne LiDAR Data

Karl Shorter

Supervisor: Heather Reese
Assistant Supervisor: Christian Öhrling

Degree project for Bachelor of Science with a major in Earth Sciences
2024, 180 HEC
First Cycle

Abstract

Airborne LiDAR (Light Detection and Ranging) is an important tool to analyze landslides in remote sensing surveys and can produce high resolution DTM's of the ground surface. By applying a multi temporal survey, it can provide information about the size, height difference and geomorphology of the landslide to better understand its kinematic and how the surface has changed. In southwestern Sweden, Quick clay landslides is common and can cause severe damage to society which means that it is important to investigate these types of events when they occur. The aim of this project is therefore to analyze and understand the movement of a recent major landslide, the Stenungsund landslide, by comparing UAV and airborne LiDAR data from before and after the landslide event. This is carried out by using different analyst tools in the GIS software *QGIS* that allows to create different models and maps of information regarding elevation difference, morphology and displacement. Fieldobservations were also conducted to support the remote sensing survey. The Results from the change analysis indicated that most of the material from the landslide has moved downhill from the upper part of the slope to the lower part and passed slope in a northwestern geographic direction. Through the interpretation of the morphology, two major flows may have caused the downhill movement due to the positioning of ridges and heaving zones. This resembles a translational progressive landslide. The study was able to understand and interpret how the landslide has moved and the extent of it, thus, future surveys have great opportunities to use UAV and airborne LiDAR in similar landslide investigations.

Keywords: LiDAR; DTM's; Landslides; Quick Clay; Change Analysis; Landslide kinematics; UAV; Airborne LiDAR

Table of Contents

1 Introduction

Light detection and ranging (LiDAR) are today regarded as an important tool to monitor and investigate landslide regions. As many other remote sensing techniques, it can collect huge amounts of data in a short periods of time, thus being a more cost-effective alternative compared to conventional field investigations (Tseng et al., 2013). LiDAR provides high accuracy 3D-models of surfaces and can produce high resolution digital terrain models (DTM) with information of the elevation. By comparing DTM's from multitemporal surveys it is possible to create DTM's with elevation differences (DoD) for change analysis studies. From this information detection of morphological features and topographical surface-change is simplified (Bossi et al., 2015b; Pellicani et al., 2019).

Earlier LiDAR applications have used Terrestrial LiDAR due to its impressive millimetric resolution (Barbarella et al., 2014; Jaboyedoff et al., 2012). However, airborne LiDAR is capable of covering a larger geographic range and can easier collect data from areas difficult to reach, in particular landslides that are still active and at risk. Furthermore, airborne methods have improved in recent years due to the development of Unmanned Aerial Vehicles (UAV's) and drones which are cheaper compared to manned aircrafts and can generate higher spatial resolution of data. UAVs have thus increased in popularity and are seen as an important tool in landslide investigations (Joon-Kyu et al., 2024; Zhuo et al., 2017).

Example of studies that have used airborne LiDAR and UAV methods for analyzing landslides is Eker et al. (2017) that conducted an UAV-monitoring of a landslide. Pellicani et al. (2019) analyzed the kinematic evolution of a landslide by comparing UAV and airborne-derived DEM's (digital elevation models). Liu et al. (2021) analyzed a reactivated landslide to understand the surface displacement and determine the type of landslide. All these studies have high resolution data (<1 m) However, most of these studies use UAV-photogrammetry and compare's it with LiDAR from manned aircraft's, which can lead to difficulties in obtaining accurate ground surface values in regions with vegetation. Thus, it would be of great interest to conduct a study with UAV LiDAR data for landslide investigations.

On the 23rd of September 2023 a massive landslide occurred during the night on the main highway E6 in the Municipality of Stenungsund, Southwestern Sweden. There were no fatalities and only a few minor injuries, however the highway and nearby buildings were damaged and are now closed off (SVT Nyheter, 2024). This has caused and will continuing to cause in major economic consequences, mostly due to extended times for vehicles to reach their destinations (Johansson, 2009). Figure 1 shows the landslides impact on the highway (Länsstyrelsen n.d.).

Quick clays are common in southwestern part of Sweden and are found in marine sediments that have been raised above sea level due to deglaciation and isostatic uplift (Andersson-Sköld et al., 2005). When quick clays are disturbed by external stresses caused by anthropogenic or natural factors, the physical structure in the sediments can easily collapse which can cause liquefaction and major landslides. Due to this, quick clays have caused great damage with one example being the 1977 Tuve landslide and most recently the Småröds landslide further north up the E6 Highway (Hartlén, 1984; Johansson, 2009). Due to the regular occurrence of landslides in this part of Sweden, it is of great importance to investigate these types of hazards when they occur.

Figure 1 *An UAV-image showing how the landslides has dislocated the highway E6 from its original place (Länsstyrelsen, n.d).*

1.1 Aim of Investigation

The aim of this thesis is to investigate the Stenungsund landslide by analyzing high resolution airborne LiDAR data produced from before and after the landslide event. Evaluating how the surface has moved and changed between these datasets provide better understanding too how the landslide behaves and to what extent it has affected the study area. To complement the change analysis, field observations will be conducted to gain a greater understanding of the study area and to compare and see if the LiDAR data resembles real field conditions. The ability to interpret and understand the Stenungsund landslide based on LiDAR will hopefully provide better insight into how remote sensing techniques can be used for future investigations in this region. Additionally, in combination with field observations this will hopefully enable a more efficient and in-depth survey. The aim is to answer the following research questions:

- Through the usage of LiDAR data, how has the surface in the study area spatially changed from before to after the landslide and how much of the landmass has moved?
- What morphological features can be detected in the landslide?
- Can the Change analysis provide information about the kinematic evolution and what type of landslide the Stenungsund landslide is?

1.2 Background

1.2.1 Airborne LiDAR and DTM

LiDAR is an active remote sensing technique that generate energy and sends out laser pulses from a sensor towards Earth's surface to calculate the elevation of ground features (Campbell, 2022). The pulses become backscattered by various objects (ground surface, vegetation, buildings etc.) to the receiving part of the sensor (Jaboyedoff et al., 2012). The sensor can thus record and measure the time of flight or time interval (Δt) described in Jaboyedoff et al. (2012), and compute the distance (d) by the equation (EQ.1):

$$2 \times d = c \times \Delta t. \qquad \text{(EQ.1)}$$

To retrieve the positions of different objects, the line of sight (LOS) direction must be known that provides information about what objects on the ground that are visible to the sensor.

Secondly a GPS must be mounted on the airborne source to know the geographic location; and thirdly, an Inertial measurement units (IMUs) is required that has precise recording of the airbone platform's orientation (pitch, role and yaw) (Campbell, 2022; Jaboyedoff et al., 2012; Lato et al., 2010). If these three are well integrated, position of the surface relative to the sensor can be determined (figure 2) (Campbell, 2022). The distance to known positioned objects enables highly accurate mapping of topography, bathymetry and objects on the Earth's surface (e.g. vegetation). It is for this reason, LiDAR is regarded as a widespread application in earth science with increasing publications relying on it over the past two decades (Okyay et al., 2019).

The advantage of LiDAR compared to other techniques is the ability to penetrate trough intermediate-range objects by receiving multiple backscattered pulses from one emitted pulse, allowing LiDAR to create models of the bare surface. Other cheaper methods such as photogrammetry and structure from motion techniques can also create models of the bare surface, however, are only suitable in cases with sparse vegetation (Telbisz et al., 2016).

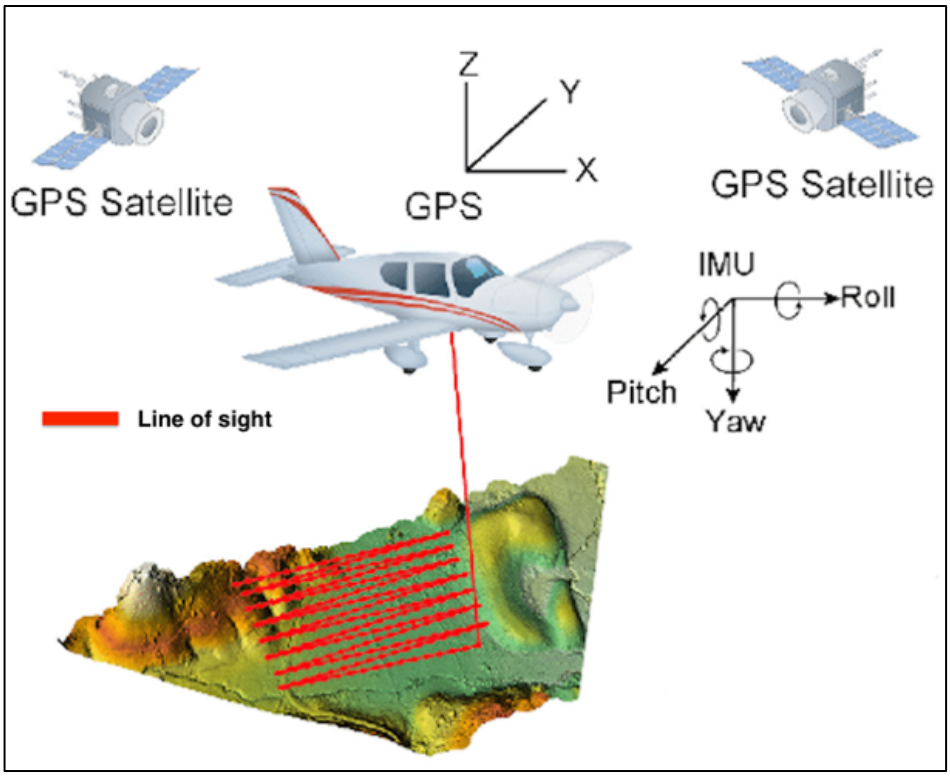

Figure 2 *A simplified illustration of LOS, IMU and a GPS device required to determine the position of various objects (Shih et al., 2008).*

The LiDAR-derived data is normally composed of three-dimensional coordinates of points known as a point cloud which can have accuracy up to sub decimeter (Mora et al., 2018). By filtering and extracting ground points from the point cloud through different mathematical algorithms and interpolation steps, high resolution DTM (digital terrain model) of bare surface can be produced to construct a 3d-model (Razak et al., 2013; Yunfei et al., 2008). This includes steps such as classification of point into ground points and non-ground points (e.g. buildings and trees) which should be carried out by carefulness since extracted points have a direct impact on the quality of DTM. It should however be considered that there can be some difficulties when generating a DTM. Examples such as dense forest, high surface roughness, preservation of sharp ridges can deteriorate the quality of the DTM (Razak et al., 2013). There have been a lot of attempts over the past years to improve the quality of DTMs and in difficult terrain situation it can still be challenging to gain accurate data (Chen et al., 2017). it is therefore important to evaluate the generated output (Razak et al., 2013).

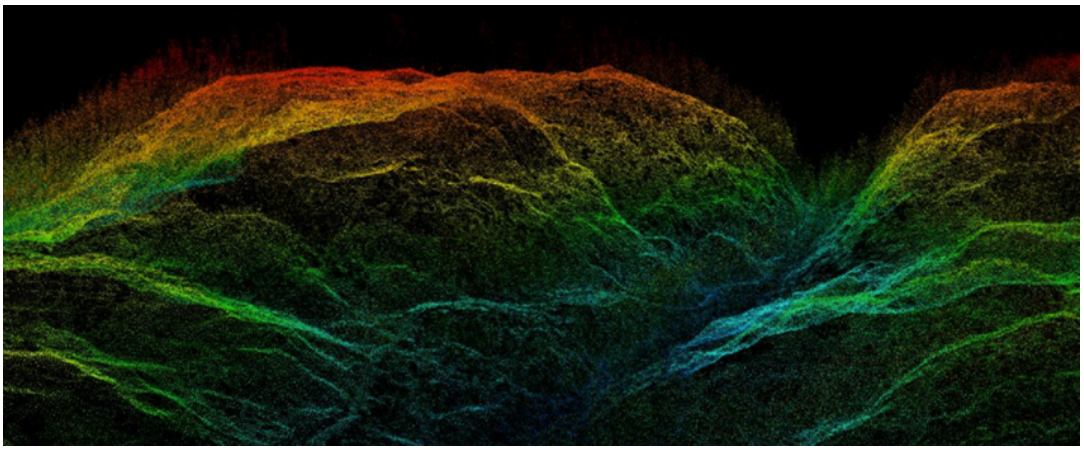

Figure 3 *Three-dimensional view of a LiDAR point cloud. The multicolor band represents the distribution of the elevation in the point cloud (Lantmäteriet, 2022).*

1.2.2 DoD Change Analysis

DoD was first introduced 1994 trough multitemporal topographic surveys to compare DTM's and detect surface deformation and change of elevation, hence, reflecting the spatial and temporal processes of landslides (Mora et al., 2018). DoD allows also the identification of the depletion and accumulation zone of landslides that can identify the morphologic evolution of surface roughness, scarps and cracks, and estimate the volume (Bossi et al., 2015a). This can be crucial information to experts such as engineers in order to prevent failure and build stable

structures (Chen et al., 2014). The survey from Pellicani et al. (2019) is an example of a recent study that used DoD analysis and stretched gray-scale images which highlighted clearly the appearance of the landslides different properties.

Volume analysis in DoD methods has recently also been regarded as an important property and can be used in risk assessments, stability analysis and detection of secondary landslides. To calculate the volume can be challenging due to the geometric information concerning slope failure surface, irregular sub surface and the thickness and height of deposits (Chen et al., 2014). DoD methods and the ability to calculate the elevation difference between pre- and post-landslides DTMs have however improved analysis of volume and many surveys use this method today (Chen et al., 2014). Figure 4 shows an illustrative example of DoD (Lato et al., 2016).

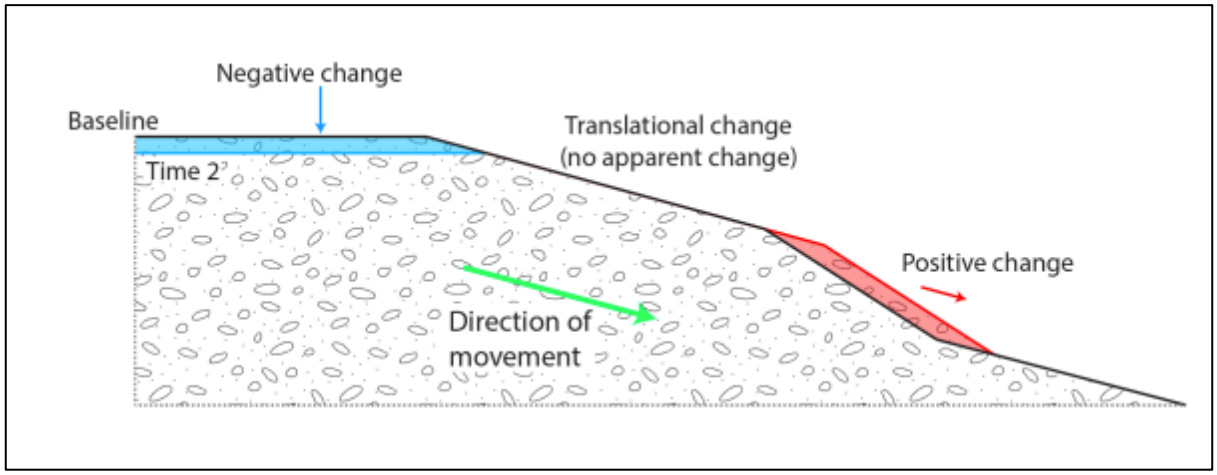

Figure 4 *DoD example of Landslide illustrating the positive change (accumulation zone) and negative change (depletion zone) with respect to a baseline (Lato et al., 2016).*

1.2.3 Airborne Vehicles

Airborne vehicles are frequently integrated in landslide analysis and gives us possibility to study areas of different sizes and scales. Extensive use of UAVs have been noticeable in the past decade and is increasingly used in environmental applications (Fernández et al., 2016). Decreasing prices have also made UAVs affordable and due to the enhancement of new algorithms in computer visions, dense matching and structure from motion approaches, this method has become a very user-friendly and reliable approach in Earth Sciences (Fernández et al., 2016).

There are different types of UAV's depending on type of survey but the most versatile is the quadcopter (Campbell, 2022). Quadcopters are powered by two pairs of rotors positioned on the outer parts of four arms. Quadcopters are extremely maneuverable and can operate in closed spaces which makes it very versatile compared to fixed wing drones. UAV's systems have also normally inbuilt programs that can plan flights in detail and optimized coverage during the survey. This makes it very user-friendly and saves time (Campbell, 2022).

Manned aerial aircrafts or fixed wings is one of the more traditional vehicles for airborne remote sensing and is still considered today when planning a survey. It can either be fixed wing (airplanes) or helicopters, having the advantages of long flight range and ability to carry various sensors and heavy loads. However, due to the cost and maintenance of manned aerial aircrafts, it has become more common to use remote-controlled platforms and UAV's. UAVs have historical roots in military action, but nowadays it has branched out more into civil applications and operations regarding environment (Campbell, 2022).

1.2.4 Formation of Quick Clay

Quick clay is a sensitive clay commonly found in Scandinavia, North America, and Russia. In Scandinavia, quick clay is mostly developed in glaciomarine sediments that was partly covered of marine or brackish water during the deglaciation of the Fennoscandian ice sheet 14000 to 10 000 years ago (Salas-Romero et al., 2016). The ablation from the ice sheet released high amount clay and silt particles that flocculated in the marine environment and formed clay-rich sediments with high water content. These sediments were later deposited on crystalline metamorphic terrain (Andersson-Sköld et al., 2005; Salas-Romero et al., 2016). The high-water content is a typical condition to form quick clay (Salas-Romero et al., 2016).

Uplift and isostatic rebound of the crust which resulted from the deglaciation, later caused coastal and low-lying areas with high amount saltwater-deposited clays to raise above sea level (Bäckström & Linder, 2021). This led to natural freshwater infiltration and circulation from rainwater and groundwater in the clay which caused leaching of salts and change in the ionic composition (Bäckström & Linder). The leaching of salts could either depend on percolation downwards trough the sediments due to surface-runoff. Or by artesian pressures which forces

groundwater to the surface and normally happens due to infiltration of water in a permeable sediment on the hillside. This infiltrated water is thereby transported down to the central and bottom part of the valley, where artesian pressures can start develop (L'heureux, 2012; Rankka et al., 2004).

The leaching may cause the clay to become sensitive to external stresses and the chemical bounding could easily collapse, resulting in liquefaction and shear strength of the clay reduced to almost zero. It is also common for quick clay to have organic content, which also affects and lower the strength. (Rankka et al., 2004; Salas-Romero et al., 2016; With et al., 2022). There are various factors that can cause the quick clay to collapse, and it is usually a surprise when it happens. Longer periods of heavy rainfall, or human factors such as construction works and landfills are examples that could disrupt the quick clay (Torrance, 2012).

1.2.5 Landslides Observed in Sensitive Clays

The group of sensitive clays to which quick clay belong, can be observed in four main types of landslides: 1) Single rotational slides, 2) multiple retrogressive slides (sometimes mentioned as flows), 3) Translational progressive landslide and 4) spreads (Locat et al., 2011). Rotational landslide is studied in earlier research to a lesser extent compared to the other three when it comes to sensitive clays. But in general it refers to landslides that occurs within the weathered crust along river valley slopes, in which none of the debris becomes liquid when remolded (Torrance, 2012). It is also characterized by scars of bowl-shaped forms (Hungr et al., 2014). The latter three occurs usually very suddenly and covers large areas (>1 ha) and is illustrated in figure 5. (L'Heureux, 2013). Observation of the four types can also be seen in one event (Locat et al., 2011).

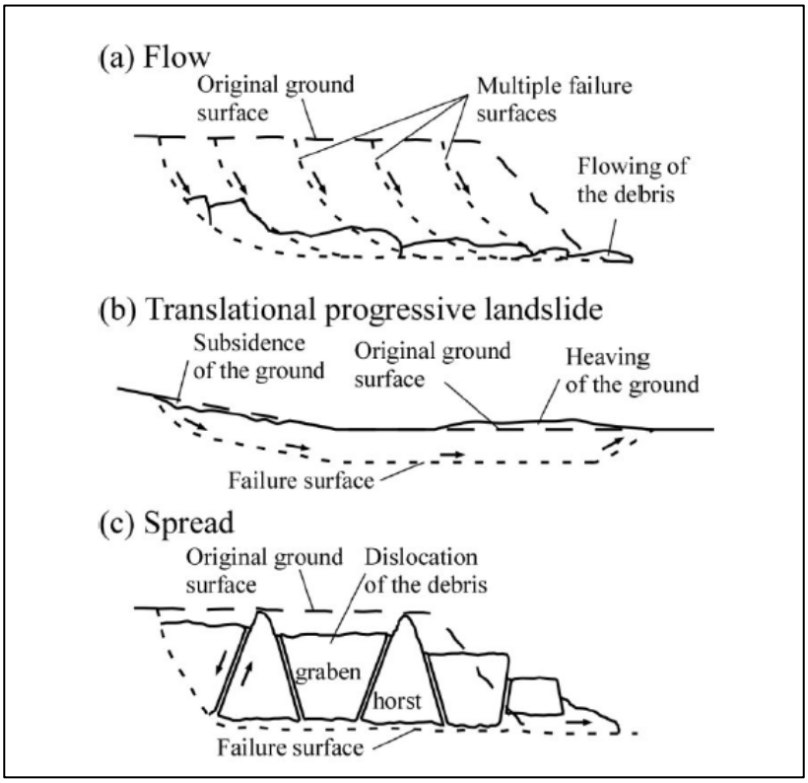

Figure 5 *Three Landslide types found in sensitive clays: a) Multiple retrogressive slides or flows, B)Translational progressive landslide and c) spreads (Locat et al., 2011).*

Multiple retrogressive landslides or flows are well described and common in Scandinavia (L'Heureux, 2013). The description of these is well documented because of the Rissa landslide in Norway, one of few Quick Clay landslides that was video recorded. Retrogression is believed to be a result from a first initial landslide which leaves behind an unstable scarp that later is also initiated (Locat et al., 2011). The landslide thus continues up the slope in a series of remolded clay flows and slides until a stable morphology is reached (figure 6), which means that the shear stress in the slope becomes lower than the undrained shear strength of the clay (L'heureux, 2012; Locat et al., 2011). The initial landslide is seen as monolithic, retrogressive, or translational and is normally triggered by stream erosion, increase pore pressure or human activity. Pore pressure increase may also be due to human activity such as pile driving, placement of fill, and leakage from utility lines (L'heureux, 2012). It is also characterized by an empty crater and has scars that are either bottle necked or progressed in direction other than directly into the slope (L'Heureux, 2013; Locat et al., 2011).

The sediments that are part of this type of landslide have generally thick layers of quick clay, a high liquidity index, and a setting where the available gravitational potential energy is sufficient to remold most of the quick clay above the failure plane (Torrance, 2012). The liquification must be sufficient enough in order to transport overlying sediments out of the landslide scar and along the valley (Torrance, 2012). Researchers in Canada have noted that the retrogression behavior may take up to several hours to develop from the initial landslide, but when earthflows starts to develop, it can happen over a short time frame (Torrance, 2012)

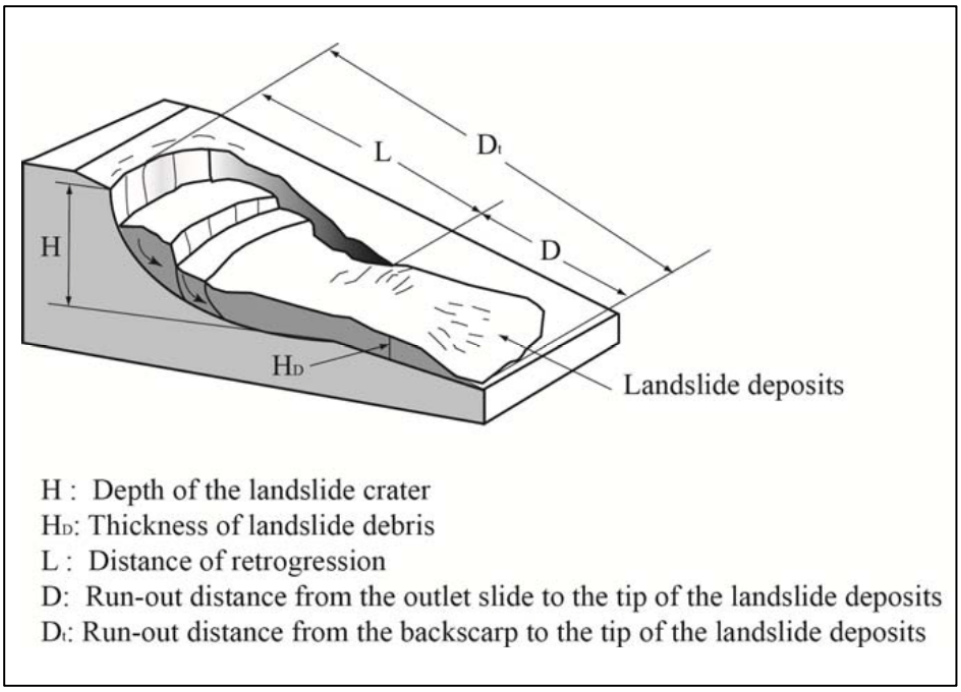

Figure 6 *A conceptual model of a multiple retrogressive landslide or flow (L'heureux, 2012).*

Translational progressive landslide is also common across Scandinavia and occurs from development of a shear surface to which material and soil masses are displaced downhill (L'Heureux, 2013). The result is a zone of depletion in the upper part of the slope and an extensive compressive heave zone down past the slope, on horizontal ground (figure 5.b) (Locat et al., 2011). The sediments are generally intact between these zones. Earlier studies have explained that the local failure in translational progressive landslides may depend on disturbances such as load filling and pilling up the slope (Locat et al., 2011). This leads to progression downhill which causes heave of a large portion of horizontal soil mass (Locat et al., 2011).

Spreads is in general more common in Canada (42 % of their large landslides) but has also been observed in Scandinavia. It happens due to extension and dislocation of the soil mass above the failure surface, in which solid-clayey horsts and grabens can start to form. These subside in the underlying remolded material forming the shear zone. The Horst blocks have a wedge-shaped form pointing upward and the graben blocks are typically a flat, horizontal top surface (figure 5.c). These forms are key to distinguish spreads from retrogressive landslides (L'Heureux, 2013).

1.3 Study Area

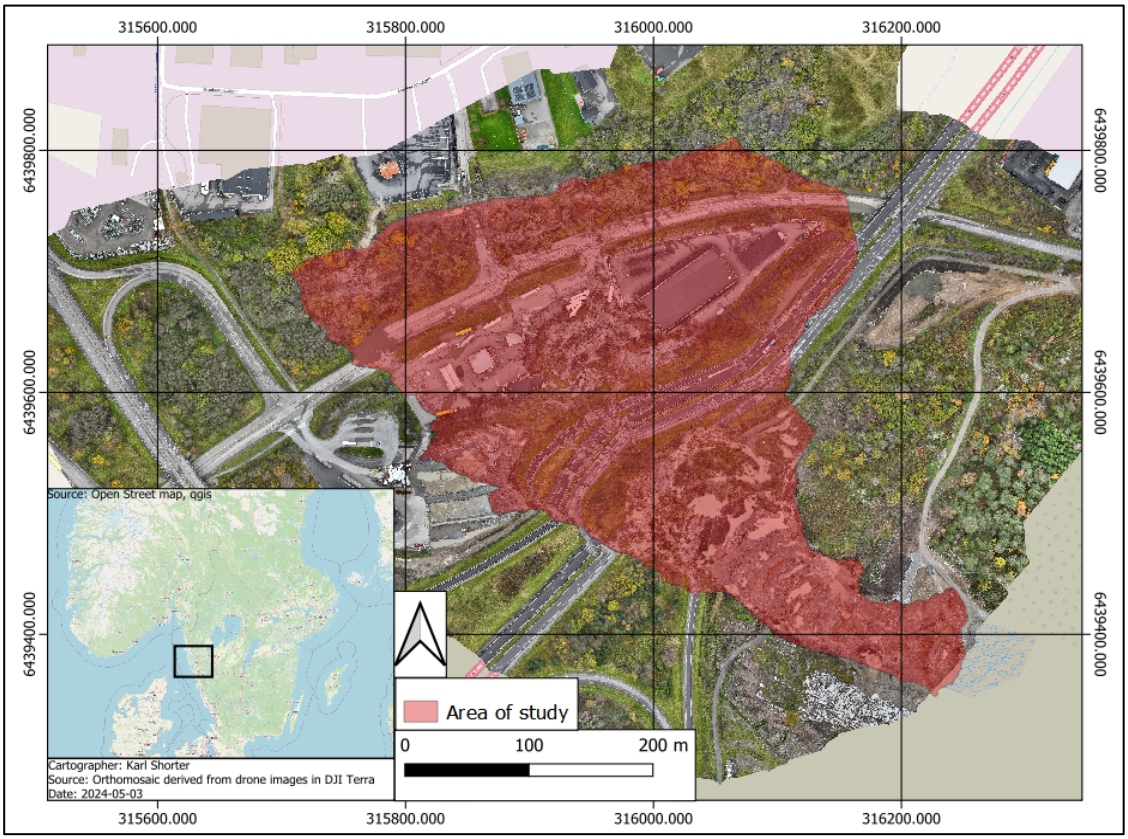

Figure 7 *Overview of the area of study (red) on top of an Orthomosaic constructed during this thesis. Most of the buildings and infrastructure is in the northwestern and lower part of the landslide area. The southeastern and upper part of the landslide is where the construction site is located.*

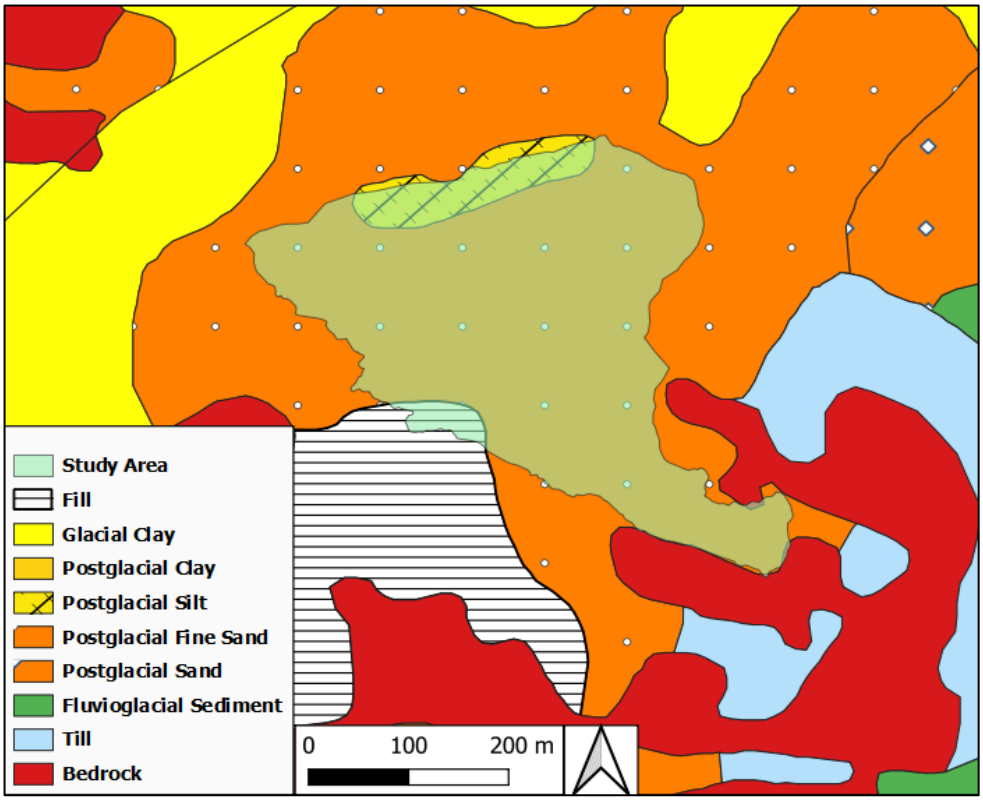

Figure 8 *Map of the sediments within and nearby the study area (transparent green). Within it consists mainly of postglacial fine sand (orange dotted) with smaller sections of landfills (striped pattern) and postglacial silt (barbed wire pattern) (Kartvisaren, n.d). The map was compiled in QGIS (QGIS, 2024).*

1.3.1 Land use

The study area is located by "Stenungsundsmotet" (by exit 91 of Highway E6), east of municipality Stenungsund (Figure 7). Besides the Highway, the area is mainly used for commercial properties, a service station and smaller roads (Byggindustrin, n.d; SVT Nyheter, 2024). A major construction site is also located in the area with a mission to build an industrial park (Sveriges Radio, 2023). The nature is made up of miner swathes of forest and a small river that is important for drainage (Svenskt Vatten, 2024).

1.3.2 Geological Setting

According to the Swedish geological survey's (SGU's) map service (Kartvisaren, n.d) (figure 8), the sediments in the study area consists of mainly postglacial sediments (sand and silt) that was carried away from ice river mouths during the deglaciation and gradually deposited on the seabed or lakebed. To the northwest and north outside the study area there is

also large amount of clay that belongs also to the postglacial sediments which represents a deeper marine depositional environment due to the finer grainsize. There are also sediments with till east outside the landslide that consists of unsorted material and was deposited from the glacier. The ice absorbed and processed older soil layers as well as material broken away from the bedrock which leads to the unsorted nature (Fredén, 1987). Bedrock (red) is also present along the surface but is not within the study area and is mainly in the southern part of the map. The sediments are therefore also relatively deep to bedrock (Kartvisaren, n.d). The depth in the northwestern and lower part of the landslide is approximately between 15-20 m and in the southeastern and upper part of the landslide, the depth becomes shallower and is between 5–10 m.

Landslide susceptibility mapping from SGU (Kartvisaren, n.d) which is based on a computational algorithm from Tryggvason (2014) indicates that the study area is an area that has the potential for landslides to occur (figure 9). The algorithm uses sediments, terrain models and critical slope (1:10=5.7 degrees) to calculate areas with susceptibility. These areas are referred to as "aktsamhetsområden"

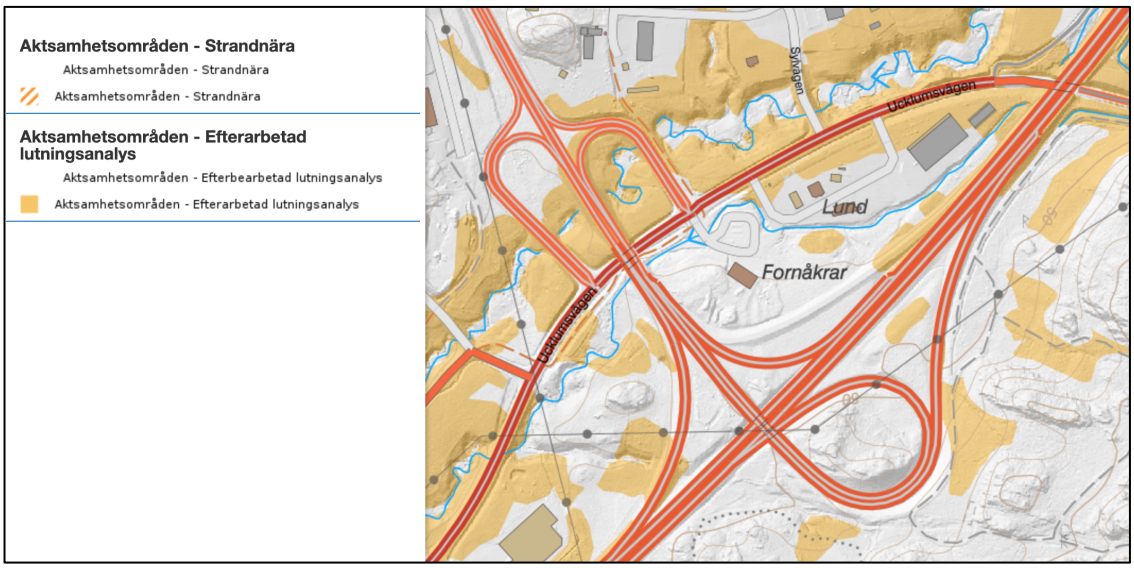

Figure 9 *SGU's Susceptibility map over the study area that indicate areas of potential risk for landslides to occur. These areas are marked in orange ("aktsamhetsområden").*

2 Materials and Methods

2.1 Data Collection

This thesis consisted of airborne LiDAR data from two different periods: one was produced before the landslide (called here the "pre-data") in 2011 and the other after the landslide (called here the "post-data") in October 2023. Detailed information about the LiDAR data is compiled in Table 1. The pre-data was produced from a manned airborne survey performed by the Swedish land survey *Lantmäteriet* who took LiDAR measurements with a point density of 1-2 points/m^2. It was downloaded as both a point-cloud (las-file) and a 1 m resolution DTM (tiff-file) using their free extraction tool (Herkules, n.d). The post-data was obtained from an UAV survey performed by the drone company *Swedron Sverige AB* who gave the thesis permission to use it. It was provided as a point-format (pnts-file) with a point density of approximately 100 points/m^2.

Orthophoto images from before and after the landslide were also retrieved to be certain that the LiDAR data represented the reality well. Orthomosaic (tiff-file) from before the landslide were also downloaded from Lantmäteriets free extraction tool (Herkules, n.d) and the images (JPG-file) from after the Landslide was also provided from Swedron Sverige AB and taken at the same time as the UAV LiDAR data.

Table 1 *Summary of the Airborne LiDAR data information from the pre- and post-data.*

Technical features	Pre-data (Lantmäteriet)	Post-data (Swedron)
Platform	Fixed wing aircraft	DJI Matrice 350 RTK (Quadrocopter)
Sensor (model)	Leica ALS60	DJI Zenmuse L2
Height of flight (m)	2200	100
Point Density (per/m^2)	~1.0-2.0	~100

2.2 Pre-Processing

In order to analyze and compare the LiDAR data, it was necessary to construct DTM's. The pre-data already had a prepared 1m resolution DTM. But to change the spatial resolution of it, which was necessary to perform the data analysis, the open-source program *CloudCompare* (CloudCompare, 2024) and the tool *LAStools* (QGIS Plugins, n.d) in the GIS-program QGIS (QGIS, 2024) were used. This process involved converting the original LiDAR point cloud into a DTM with a different spatial resolution, which was 0.25 m and 2 m. Cloudcompare's task was to subsample and minimize the number of points which allowed LAStools to handle large file size and convert the point cloud to a DTM. To construct the post-data into a DTM, the producer of the UAV and sensor, DJI Enterprise, have created the software DJI Terra (DJI Terra, 2024) that can convert points to a point cloud and DTM in few steps. DJI Terra had different settings to optimize the data for the specific purpose and was considered during the construction. The parameters were set to get as detailed output as possible, with settings such as *steep slope* to optimize the sharp elevation change of the landslide (see appendix A and B). Finally, a 0.25 m and 1m DTM's were constructed from the post-data to be able to analyze the morphology (0.25 m) and to compare and do a DoD change analysis (1 m) of the pre- and post-data. The orthophoto images from the post-data were needed to construct an orthomosaic and was also converted in DJI Terra (DJI Terra, 2024) (see appendix). Because of the large amount of data from both the pre- and post-data, a powerful computer with a dedicated graphics card was used for the processing to be carried out.

2.3 Remote Sensing Tools and Data Analysis

The data analysis consists of three main parts: (1) DoD change and volume analysis, (2) Mapping of the Landslides Morphology and Displacement and (3) Standard deviation analysis between DTMs. These three will be explained in detail in the following paragraphs. These parts were mainly performed in the GIS-software QGIS (QGIS, 2024), an open software platform with various important tools to investigate the spatial information of landslides. Before the data analysis was conducted, the area and size of the landslide was identified by analyzing orthomosaics and DTM-derived hillshades from the pre- and post-data. This step focused the analysis to the area of interest and removed data outside of the area of interest. It also provided information regarding the square surface area of the landslide.

2.3.1 DoD Change and Volume Analysis

To determine the DoD between the pre- and post-data, the built-in function *raster calculator* tool in QGIS was used. It is a tool that allows to perform calculations based on existing raster pixel values. In this case, the pixel values in the DTM's are in meters above sea-level (MASL) (QGIS Documentation, n.d). The resolution that was selected for this task was 1 m. This was due to the inaccuracy the pre-data had when using the higher resolution 0.25 m DTM due to the sparseness of the point cloud. The aim of this method is to derive a DTM with positive or negative change for each pixel depending on whether there has been depletion or accumulation on the surface. The calculation in the *raster calculator* was expressed in the following equation (EQ.2):

$$\text{“dtm\_post\_data”} - \text{“dtm\_pre\_data”} = \text{“elevation\_change”} \qquad \text{(EQ.2)}$$

By gaining information regarding the depletion and accumulation, expressions could be used to calculate the amount of volume that had been removed or added to the surface. There are different methods to implement this. This thesis tested two methods to be able to compare and ensure that the value of the volume is reasonable. The first method was conducted manually by multiplying the number of pixels with the mean value for the positive values (accumulation) and for the negative values (depletion). To separate the positive and negative values from the DoD "elevation_change", some new expressions were calculated in the *Raster Calculator*:

- "elevetation_change > 0" resulted in an output "depletion_zone" with the value 1 indicating the pixels that corresponds with the expression.
- "depletion_zone × elevation_change" resulted in an output "positive_values" that showed all the positive values in a DTM. Information about the mean value could thereby be accessed to calculate the total volume.

The expression "value <0" was used instead to produce a DTM with negative values.

The other method that was used was the built-in tool *Raster Surface volume* in QGIS (QGIS, 2023). This tool is an algorithm that calculates volume under a raster grid surface and can be controlled whether the positive or negative pixels are calculated (Geodose, 2020). The DoD change expressions was first conducted to do this method. The resulting values came in a

HTML-file. To deepen the analyses, the *profile tool* (QGIS, n.d.b) was used to plot a profile of the terrain in the DTMs. This made it clearer of how the surface spatially changed throughout the landslide area, and to determine the type of landslide.

2.3.2 Mapping of the Landslides Morphology and Displacement

Mapping of the Landslides morphology and displacement was carried out by creating and digitizing shapefiles with lines, polygons and points. The different features were categorized as either scarps, cracks, ridges, vector displacements or infrastructure (buildings, roads. etc.). Before the mapping was conducted, different DTM-derived models were produced to determine which model or models gave the clearest indication of the morphology. finally, it was clearest to compare a slope model of the DTM from the post-data with the orthophoto images to map the morphology. The slope model gave insight to how the inclination of the surface drastically changed, and this simplified the detection. The displacement was determined by comparing orthophoto images from the pre- and post-data. Identifying known objects from the images made it possible to add reference points between the images. A vector between the points was produced by the *points2one* tool (QGIS Plugins, n.d.c). The vector could thereby be used to measure the length of the displacement and the direction of movement.

2.3.3 Standard Deviation Analysis in QGIS

To understand how the DTMs resolution and accuracy affects the survey, the pre- and post-data's DTMs were compared. To do this, the standard deviation of values within different pixel resolutions of DTM's were calculated to understand how much a higher resolution deviates from a lower resolution. The test required the *zonal statistics* tool in QGIS which allowed calculation of statistics on the pixels within a determined polygon area (or "zones") (QGIS Documentation, n.d.b). In this case the statistics were calculated on the pixels from the 0.25 m DTMs that fell within 1 and 2 m DTMs pixel area. This meant that the 1 and 2m DTMs pixels was converted to polygons ("zones") via the *Raster pixels to polygons* tool (QGIS Documentation, n.d.c). The resulting standard deviation values were summarized in new shapefile outputs, at 1 m and 2 m spatial resolution.

2.4 Field Observations

Field observations were carried out for half a day together with an assistant supervisor. Notes and photographs were done over the study area to compare and get a better understanding during the remote sensing analysis. Specifically in areas that had uncertainties regarding morphological features and height.

3 Results

3.1 Change of DTM-Derived Models

This section shows some of the DTM-derived models from the pre- and post-data that describes the change between different properties of the landslides surface:

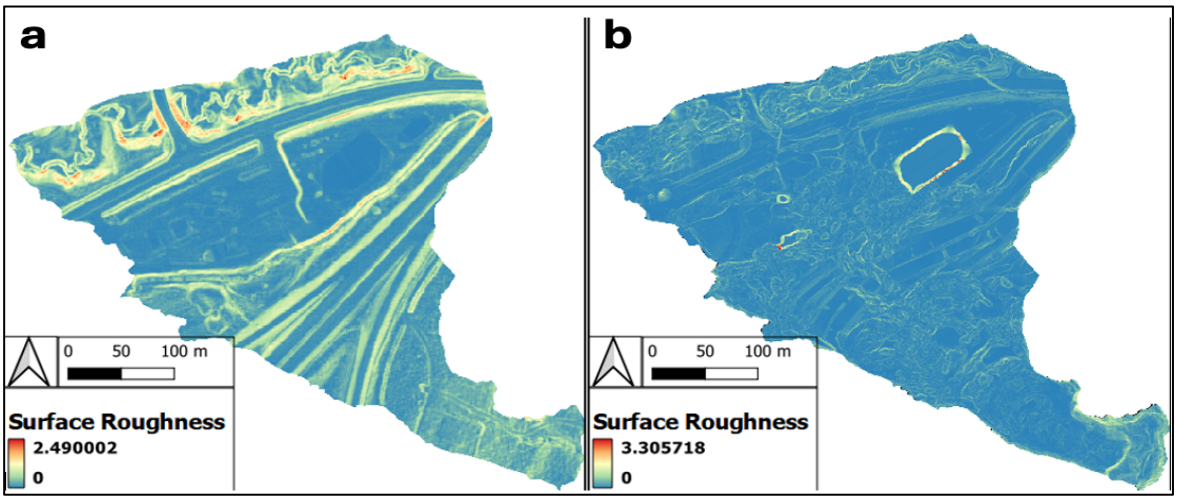

Figure 10 *Degree of irregularity on the surface (roughness). a) pre-data. b) Post-data. The pre-data has overall higher values compared to the post-data, but the post-data has the highest max value.*

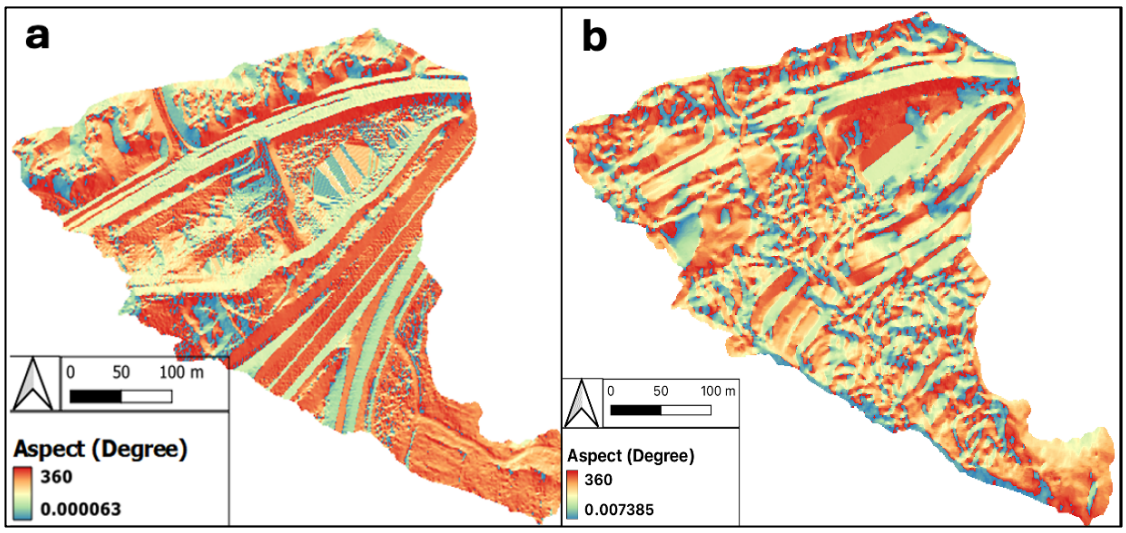

Figure 11 *The geographical orientation of the slope (Aspect). a) pre-data with larger part of the area covered by red with a northern orientation b) Post-data with a large fluctuation of orientation.*

There is no significant difference of the surface roughness between the pre- and post-data (figure 9) indicated by the surface roughness values. The pre-data (figure 10.a) has however values that fluctuate more compared to the post-data (figure 9.b), and in the northwestern part it has also significant higher values. The post-data has more even values, but it is still clear where the surface is either disturbed or intact, with yellow and red areas indicating higher surface roughness (figure 10.b)

The aspect between the pre- and post-data is significant different due to that the pre-data have a slope orientation manly to the north (figure 11.a) compared to the post-data which has a more western to southern slope direction and has an orientation that fluctuate a lot more (figure 11.b). The aspect of the pre-data (figure 11.a) indicates also how the slope shallows to the northwest where the aspect begins to have several directions compared to southeast where the aspect is mostly red and has a northern direction.

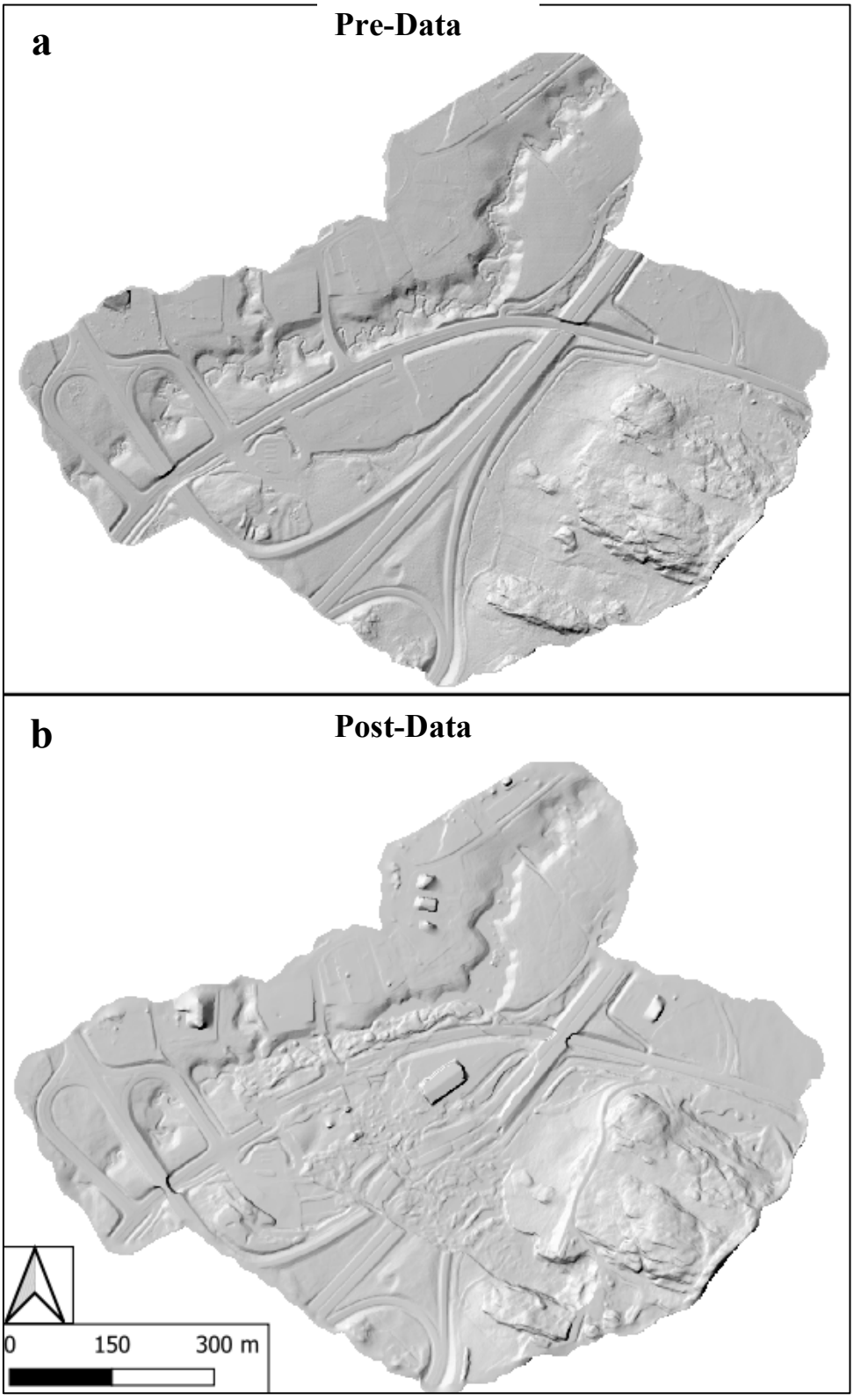

Figure 12 *DTM-derived 1m resolution hillshades. a) Pre-data that shows the intact highway and its direction. b) Post-data that shows the scar of the landslide and how it has dislocated the highway and effected the area*

The hillshades (figure 12) indicate how the landslides have massively changed the surface and have caused great damage, not only the highway in the center but also the small river that has been clogged from the accumulated material (figure 12.b). The scar also shows the extent of the landslide having a southeast to northwest direction. in the upper part of the slope (southeast) the landslide has a bottle shaped scar that widens out down the slope towards the northwest.

3.2 Identified Morphological Features and Displacements

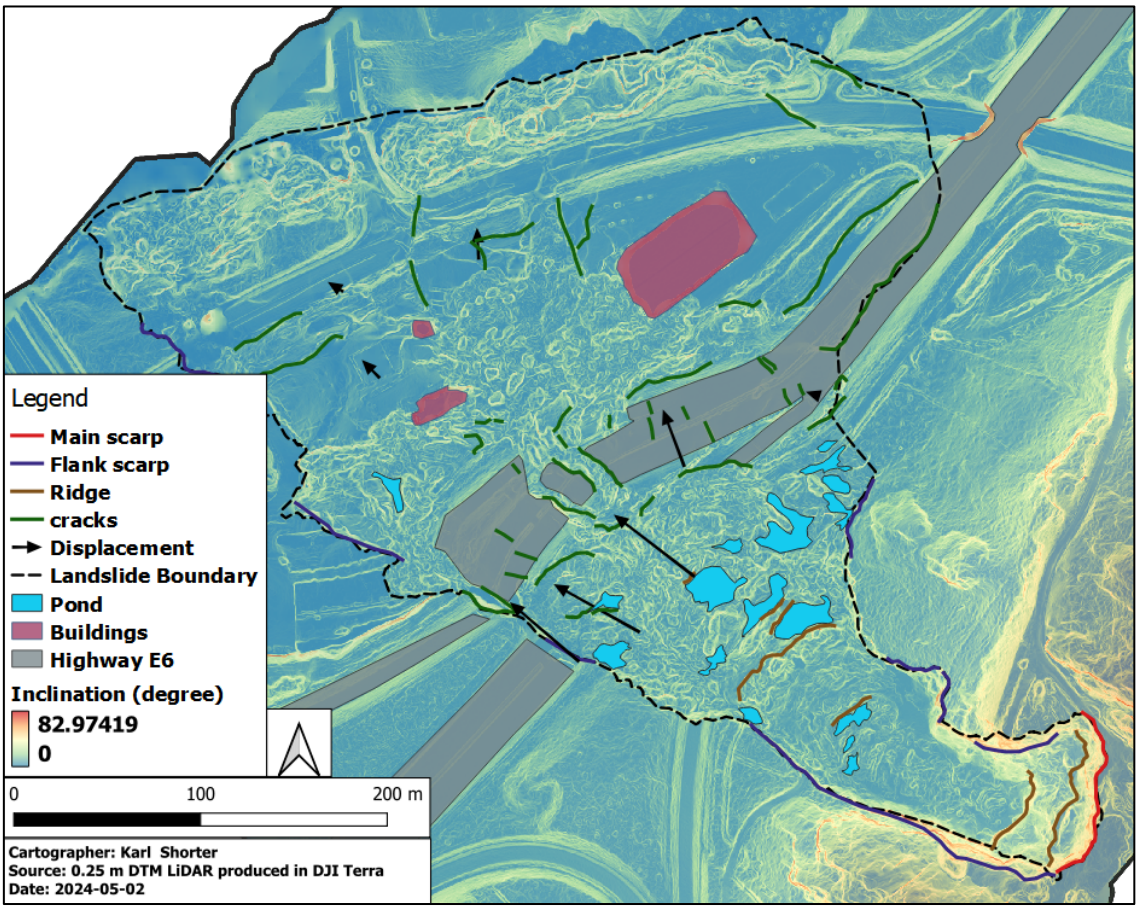

Figure 13 *Slope model (inclination) with the morphological features and vector displacements of the landslides from the post-data. The features were easiest to identify in areas with high inclination (yellow to red symbology).*

The morphological features of the landslide were manly based on the change of inclination in the study area from the post-data. The different features had a tendency to be identified in certain areas of the landslide (figure 13). The cracks are mostly located in the northwestern part where the landslide widens out and some of the buildings and infrastructure are still intact. The

ridges and ponds are instead located in the southeastern part where there is mostly debris and no intact surface (figure 13).

The displacement vectors have similar tendency as the cracks and are found nearby the affected E6 Highway but also further northwest to the end of the landslide (figure 13). The displacement vectors were depended on objects located on both the pre- and post-data which meant that buildings and infrastructure played an important role. The direction of the displacement vectors fluctuated from west to north and it is two clear main directions, one that goes to the northwest and the other that goes to the north.

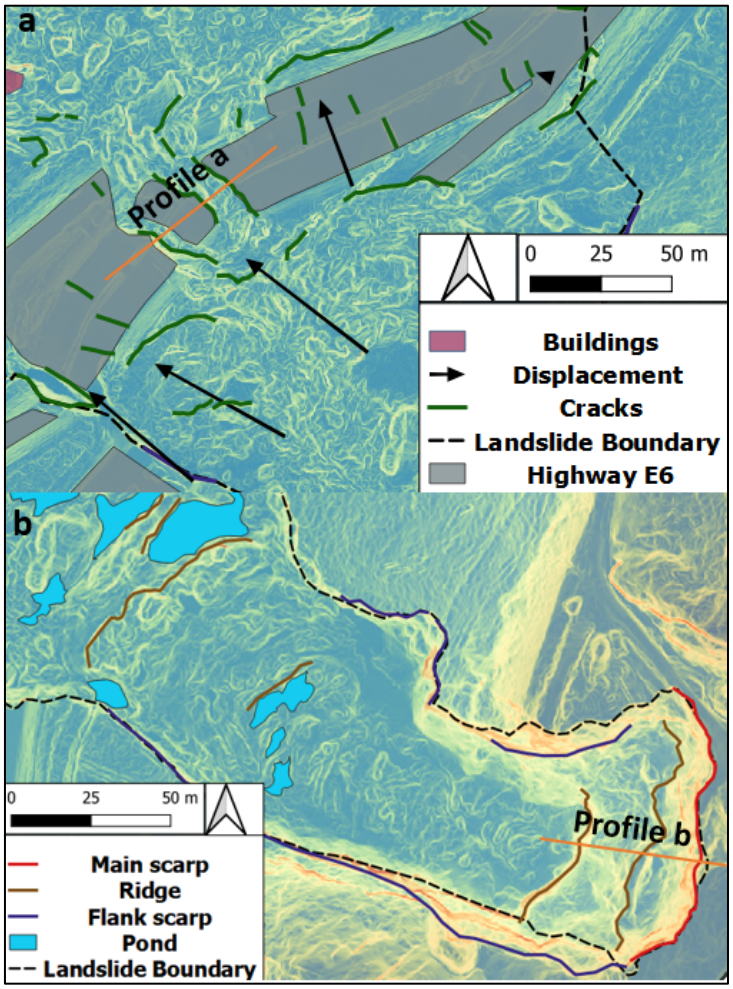

Figure 14 *Zoomed in representation of slope model and morphological features. a) A highlight of the vector displacements and the impact on the highway E6. Profile a is the location of figure 15.a. b) map over the upper part of the landslide with repeated ridges along the landslide. Profile b is the location of figure 15.b.*

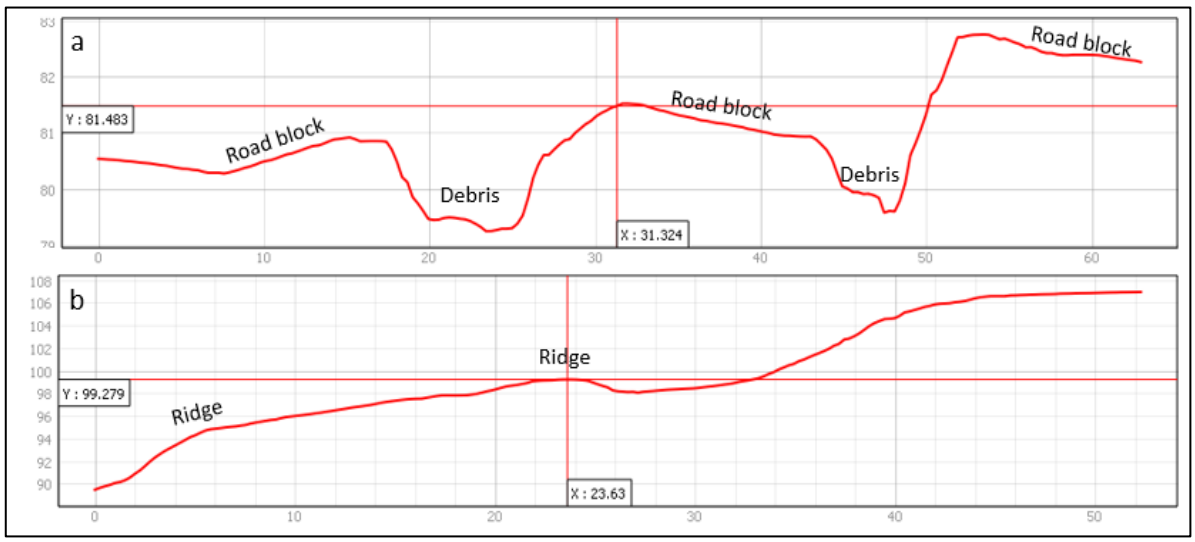

Figure 15 *Graphs containing profiles from two sections. X-axis is distance (m) and y-axis is MASL a) Profile parallel to Highway which have great elevation change as a results from the cracks and dislocation of the highway. b) Profile of the upper part parallel to the landslide with two ridges that indicate a waveformed structure.*

Figure 14 and 15 highlights two areas of the landslides: figure 14.a that shows how the vector displacement and cracks are distributed along the highway; and figure 14.b that shows the perpendicular ridges in the upper part of the landslide, close to the main scarp. These figures have a profile a and b that is illustrated in figure 15.

There is large number of cracks located on the highway and are parallel to the movement of the displacement (figure 14.a). As seen in profile a in figure 15.a, four cracks are significant bigger compared to the rest and there are the two main entrances where debris has dislocated and passed the highway. The cracks show elevation change of up to three meters (figure 15.a). As mentioned in figure 13, there is two main directions of the displacement indicated by the two vectors in the southern (figure 15.a). These directions correlate with the form of the scar which has a straight southern flank scarp but a bending northern flank scarp (figure 13).

In figure 14.b, there are multiple ridges and ponds. There ridges are perpendicular to the movement of the landslide and repeats from the main scarp down towards the ponds that are clustered in an area between the cracks and ridges (figure 14.b). profile b (figure 14.b) crosses two ridges near the main scarp that has a wave-formed (figure 15.b).

3.3 DoD Change analysis

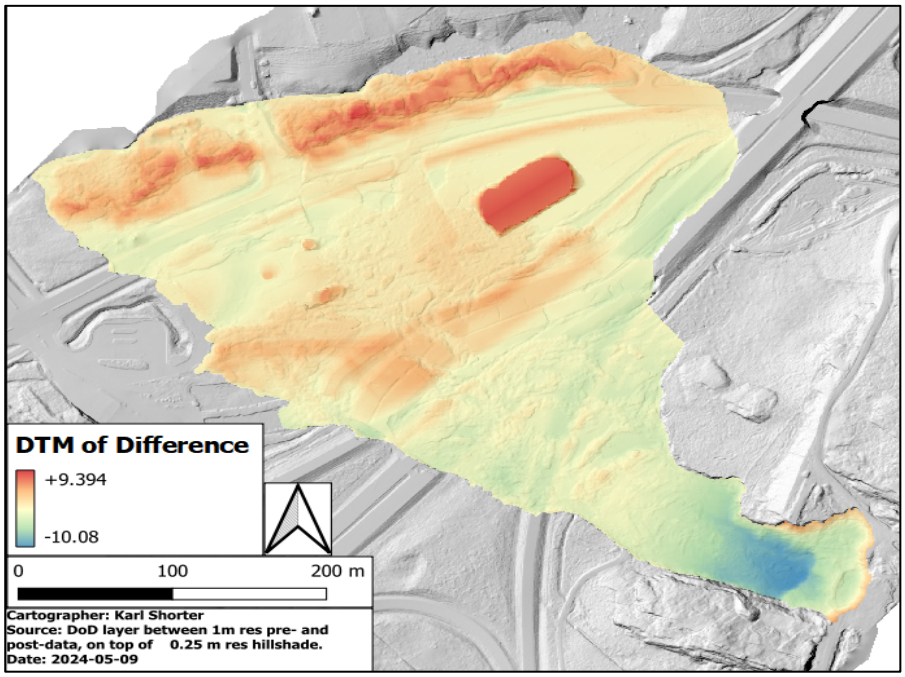

Figure 16 *DoD change model (in meters) of landslide area, placed on top of the hillshade from the post-data.*

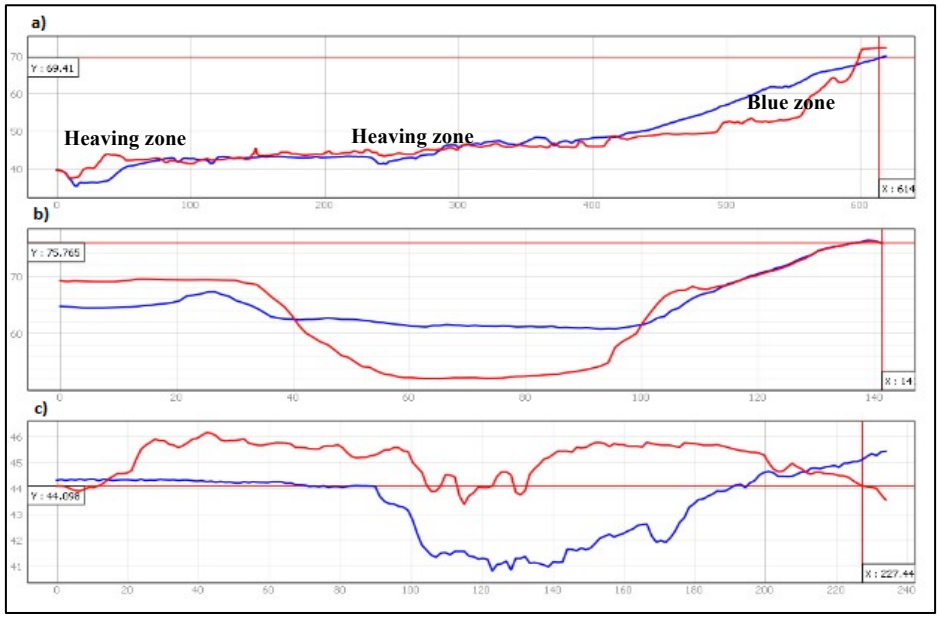

Figure 17 *The graphs represent profiles of DoD (m) between pre-data (blue) and post-data (red). a) Profile parallel to the landslide movement b) Profile perpendicular to the landslide movement and is located in the zone of decrease elevation, similar location to Figure 15.b. c) Profile perpendicular to the landslide movement and is located in the zone of increase elevation, similar location to figure 15.a.*

The results from the DOD analysis shows an elevation difference of up to 10 meters (figure 16) and there is two main zones clearly noticeable. A zone with positive values in the northwestern part that indicate increase in elevation, and a zone with negative values in the southeastern part that indicate a decrease in elevation. In the zone with increase elevation there seems to be two areas with higher values (red zones) and has a ridge-shaped heaving form perpendicular to the landslide's movement. These two heaving areas are highlighted in figure 17.a and are located near the highway and the water stream. The zone with decreased elevation have also an area with higher values (blue zone) and is also highlighted in figure 17.a. This zone is located near the main scarp. Figure 17.b-c is profiles that shows height difference between the pre- and post-data. The height difference can be up to 10 m in certain areas. Finally, it must be clarified that the red box in figure 16 is a building which could not be removed during the filtering and construction of the post-data's DTM, and it is therefore high positive values in this area.

3.4 Calculated Size and Volume

Table 2 *Summary of the size and volume from the decreased- and increased elevation. Values calculated from DoD and the raster surface volume tool.*

spatial features	Negative zone	Positive zone
Average DoD (m)	1.7219	2.2212
Area (m^2)	53 396	63 452
Volume (m^3)	91 944	140 387
Subtract false DoD		119 977

Table 2 contains the values of area-size (m^2) and the volume (m^3) that has been added or removed from the two zones of positive and negative values. The row *Subract false DoD* is a step that was added to remove the building from the negative values to ensure that the volume is true for the negative values. The area size of the landslides was calculated to be 116 848 m^2. The positive zone (accumulation) is larger in area compared to the negative zone (depletion) and this was also the case for the average DoD. Hence, the volume of the negative zone is also significantly larger than the depletion zone.

3.4 The Standard Deviation Between DTM's

Table 3 *Standard Deviation between different DTM Resolutions.*

Zonal layers	Standard Deviation (m)
0.25 m UAV, 2m Lantmäteriet	± 0.099
0.25 m UAV, 1m Lantmäteriet	± 0.051
0.25 m Lantmäteriet, 1m Lantmäteriet	± 0.045
0.25m Lantmäteriet, 2m Lantmäteriet	± 0.089

The standard Deviation between lower resolution with higher resolution data does not reach above 0.1 m for every DTM that is compared. The values are larger if the difference in resolution is larger. Same outcome is reached for both the pre- and post-data with different resolutions (table 2).

3.5 Field Observations

The study area had changed a lot since the post-data was taken in autumn 2023. The field observations were carried out 16th May 2024 by taking photographs from different position and angels that were useful for the thesis. much of the surface and material has unfortunately been moved by trucks to be able to rebuild the highway but also due to safety concerns. This meant that the field observations did not have a large part in this study as it was not comparable with the Lidar data. There are however some areas that are relatively untouched, and these have been included in the survey (figure 18-20).

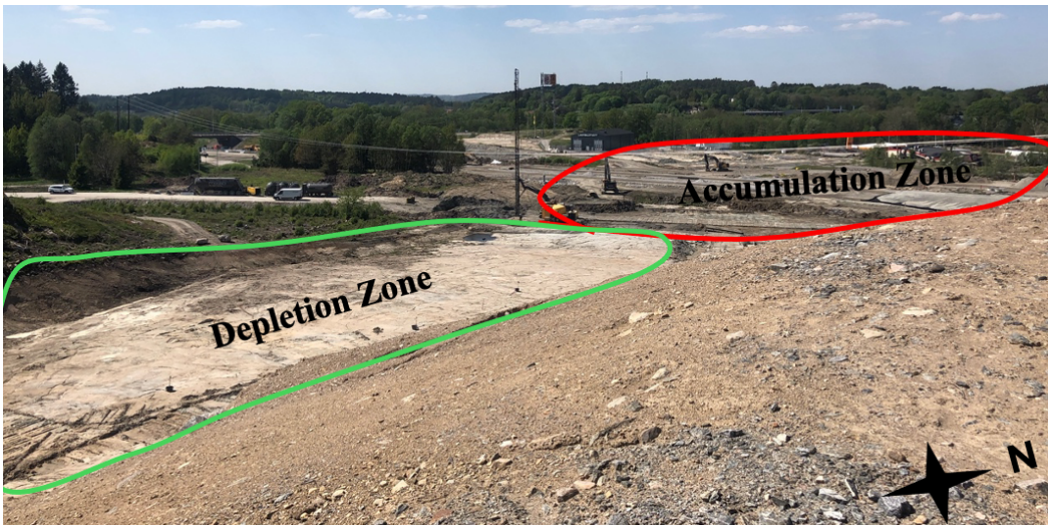

Figure 18 *Photograph taken from the Northeastern part of the study area which provides a good overview.*

Figure 19 *Photograph of the main scarp which shows that a large amount of material was removed when the landslide occurred. It also gives information about the influence that the bedrock had on the scars shape.*

Figure 20 *Photograph taken in the northwestern part of the landslide. This shows the impact that the landslide had on buildings and infrastructure. One of the heaving zones are also part of the image.*

Some of the features that were observed from the remote sensing studies were also identified in field. For example, Figure 18 which displays the two zones could be compared with the DoD change analysis (section 3.3). It is clearly visible that material has been added and compressed to the right in the upper part of the image (marked as accumulation zone). To the left of the image is a flat area that is at a lower level compared to the surrounding terrain and this is where material has been removed (marked as depletion zone) (figure 18). Figure 19 shows where the main scarp is placed but it is difficult to know if the appearance have changed since the post-data was produced. It is bottle shaped similar as the LiDAR data and it consists of loose sediments. The bedrock is however highly linked to the scarps shape as seen in the top right corner. The field observations also show the clear impact that the landslide has had on buildings, infrastructure and the nature in the study area (figure 20). The right part (figure 20) indicates how trees have been displaced and moved from its original position. This is also the case for the buildings that have been displaced in an angle and some are even covered in debris. Heaving zones was identified and one of them is placed nearby the white-red building to the right in the image (figure 20). This heaving zone is perpendicular to the movement of the landslide as previously seen from the LiDAR data.

4 Discussion

The analysis of the LiDAR models that were produced from the pre- and post-data in QGIS clearly shows that there has been a large change in the surface between before and after the landslide. The values and surface in the post-data is in general more irregular compared to the pre-data. An example of this is the surface roughness (figure 10) and the aspect (figure 11) in section 3.1. However, when it comes to the values of the surface roughness, the post-data did not have significant higher values after the landslide as could be assumed due to the scar that the landslide leaves behind. What this may be due to is difficult to say but could be related to differences in how the pre and post data have been produced. The aspect that the post-data had has not as clear direction of the slope compared from the pre-data which may mean that the slope has partially been even out and sunk.

When analysing the height differences, the DoD change analysis shows that there is up to 10 meters differences in height between the pre- and post-data. This is clearly seen in the DoD change model and the comparing profiles (figure 16 and 18). Furthermore, the DoD shows that a large amount of the mass has moved from the southeastern to the northwestern part due to the negative values (decrease in elevation) in the southeastern part and the positive values (increase in elevation) in the northwestern part. This resulted in a displacement of large amounts of land mass as shown clearly when analysing the volume and thus it has been possible to divide the landslide into a depletion and accumulation zone. The values from the calculated volume shows that there is more volume added in the accumulation zone compared to the volume removed in the depletion zone. It is difficult to determine the reason for this. In part, this may be due to that the accumulation zone in the post-data had included the building in the point cloud and thus it is possible that there are several other points that are incorrect which have not been identified. But it could also be due to the dynamics of the landslide that has caused the removed volume in the depletion zone to push up the already existing surface in the accumulation zone. This has contributed to more volume being calculated than has been added in the reality.

4.1 Interpretation of Landslide Type and Kinematics

By comparing the DoD change, profiles and the morphological features, the Stenungsund landslide is assumed to be a translational progressive landslide. The analysis suggests that most of the material from the surface is displaced downhill. In particular when analysing the DoD change model and profiles. It is also clear that the DoD change consists of a zone with extensive compressing heaving material further down the slope and a zone of depletion in the upper part of the slope which this type of landslide is characterized as (L'Heureux, 2013).

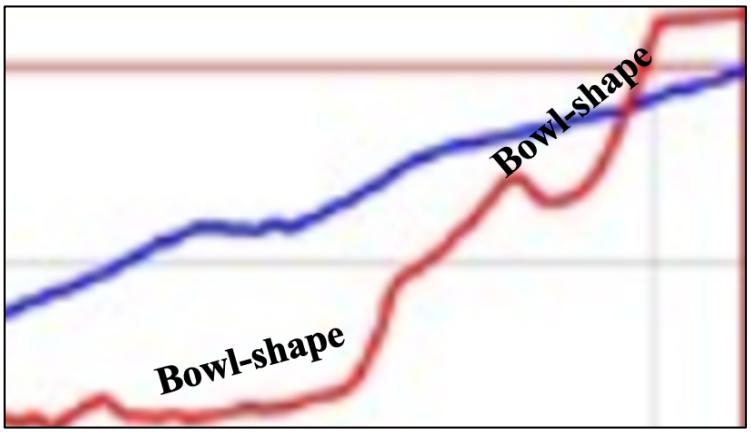

Figure 21 *Bowl-shaped forms similar to rotational landslides. Zoomed in image of the parallel profile to the landslide*

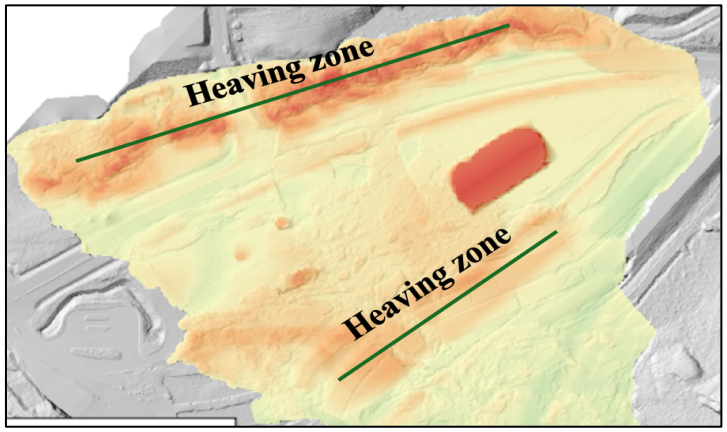

Figure 22 *Extreme Heaving zones from the DoD analysis*

When comparing the profiles between the pre- and post-data (figure 17) with the types of sensitive clay landslides illustrated by L'heureux (2012) (figure 5), it was however not as clear to interpretate. This was due to the different characteristics that were found in the results.

Firstly, the upper part of the landslide (figure 21) consisted of two repeated bowl-shaped forms with ridges indicating the boundary between them. The bowl-shaped form is normally associated with rotational landslides, the type which is not as common to be found in sensitive clays (Hungr et al., 2014). The repeated characteristics could also be scars of multiple slides which could also be an indication of a multiple retrogressive behaviour (L'heureux, 2012; Locat et al., 2011; Torrance, 2012). The accumulation zone is not completely homogeneous and has two specific areas where the heaving is more intense (figure 22). These two zones could potentially be linked to the retrogressive behaviour with multiple flows compressing the accumulation zone thus, from the interpretation, there might have been two major flows during the landslide. It should however be considered that the landslide did not likely start in the lower part of the slope which usually occurs in retrogressive conditions. Most material is transported and accumulated further down and past the slope in the accumulation zone (L'heureux, 2012; Locat et al., 2011). The ponds that were mapped gave no clear indication of the type of landslide or how it moved. But it does indicate that many pits have been created from landslide scars where water has been filled.

According to the displacements and direction of vectors, the landslide seems to have two areas along the highway where the southern vectors tend to have directions more to the west compared to the northern vectors that have a direction more to north (figure 14.a). The highway's timing of cracks and dislocation can perhaps have contributed to this. It is also interesting to see a similar pattern of the vector's direction and adjacent cracks. The fact that the slope levels out towards the centre of the landslide could also have had an impact, which means that the debris could have started taking different paths. However, it should be made clear that one part of the highway has been bent and has not separated completely from the original position. If instead the part of the highway had been separated directly, the bending of the highway may not have occurred, and the direction of the northern vectors would be different.

The extent and movement of the landslides is towards north to northwest direction downhill according to the post-data and the landslide scar. The direction seems reasonable when compared to aspect (figure 11). The scar in the upper part of the slope is relatively narrow which may be due to the adjacent bedrock which is seen on the DTM-derived hillshades, Kartvisaren (n.d) and from the field observations. This may hinder lateral extension of the landslides. Further down the slope, however, the landslide begins to spread laterally but mainly

on the northern flank. The southern flank maintains its straight line all the way to the end of the landslide. This may be due to the direction of the aspect but also the continuation of the bedrock adjacent to the southern flank.

4.3 Discussion of Materials and Methods

The result of this study supports the high potential of the use of LiDAR-derived DTMs for landslide analysis that were mentioned in earlier studies (Bossi et al., 2015b; Chen et al., 2014; Mora et al., 2018; Pellicani et al., 2019). The methods were easy to understand and time-efficient. The DoD change and volume analysis required short amount of processing time to derive a large amount of data. The volume was calculated both manually and by a QGIS tool, which had identical values meaning that these two methods probably calculated in the same way. The Identification of morphological features and displacement were firstly intended to be implemented by comparing the pre and post-data of the DTM's and to use grey-stretched scale images as Pellicani et al. (2019) did. This method worked partly, and some features were very visible. However, other input data and tools were also tested and displayed more features. The slope model was the best model and was instead mainly used during the mapping. It is thereby of importance to use different images and tools to capture features but also determine model's that are most suitable for the type of study (L'heureux, 2012; Locat et al., 2011). Ponds and cracks were difficult to identify which made orthomosaics a good compliment for the analysis.

The pre- and post-data were produced by different survey as previously mentioned, which resulted in differences in the accuracy and resolution between them. The post-data from Swedron that was captured from an UAV have considerable higher resolution of LiDAR-points compared to the aircraft survey from Lantmäteriet. The UAV-derived data was hence much more efficient to analyze which simplified the identification of morphological features (Figure 23 and 24) (Joon-Kyu et al., 2024; Zhuo et al., 2017). The DoD change analysis was first intended to use 0.25 m resolution, but due to the sparse density of the pre-data, it became distorted and less interpretable which meant that 1m resolution was used instead. From the Standard deviation between DTMs (table 3) there might however not be much of a difference in the values between the resolutions. Thus, the lower resolution has probably not affected the final result of the DoD change analysis.

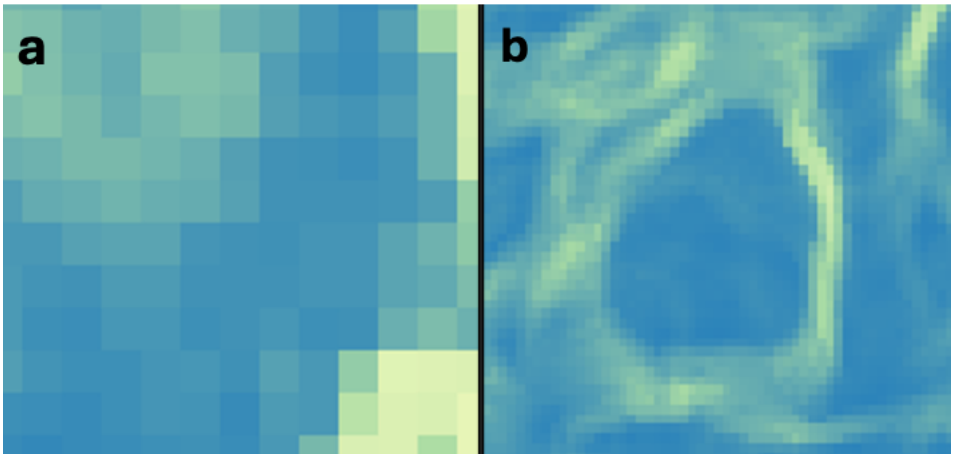

Figure 23 *Comparison of resolution in the slope-model. a) Pre-data. b) Post-data.*

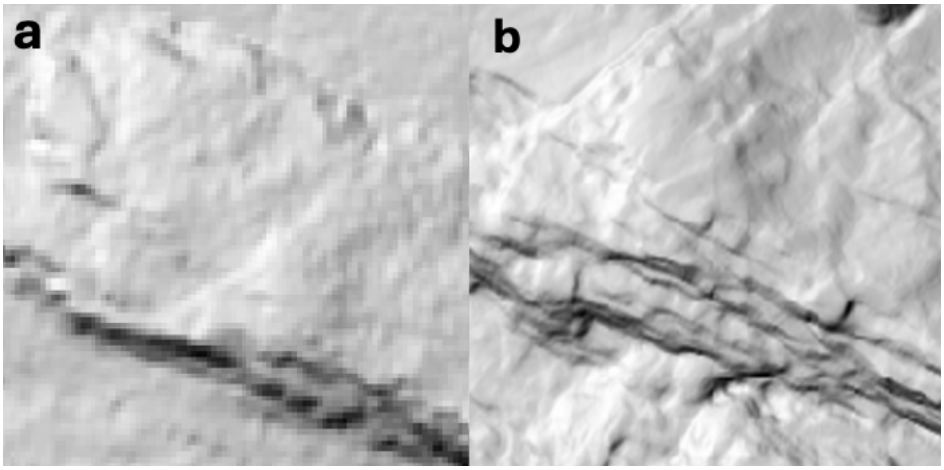

Figure 24 *Comparison of resolution in hillshade-model. a) pre-data. b) Post-data.*

4.5 Uncertainties and Further Research

The thesis has proven that the conducted methods have worked to some extent but there are some steps that could have been taken more into account during implementation. The DTM's between the pre-and post-data were reconstructed by different tools which are unlikely to use the same algorithms. This was due to the difficulties in reconstructing the large amount of data from the post-data in CloudCompare. The processing time took extremely long and the resulting DTM had incorrect pixels compared to a DTM constructed by DJI Terra. The DJI reconstruction was also not perfect and failed to remove some points belonging to objects and

buildings. This caused difficulties in analyzing the volume. This error could be due to the type of camera sensor on the UAV or software issue. It is therefore important to learn and understand the characteristics of camera sensors and software's before an investigation can begin. A future task could also be to identify a reliable program that can handle point clouds with varying density.

Remote sensing has proven to be an effective tool in this thesis, but it has also shown that field observations should always be considered when dealing with landslides. Characteristics such as structure geology and geochemistry could further developed the interpretation of kinematics and would be interesting to investigate in field. The few field observations made in the form of pictures and notes were very helpful and provided valuable information for interpreting the landslide and the change in the pre- and post-data. But due to the change that had occurred in the study area since the post-data was taken, it limited the field observations. Another parameter that could have been considered and may be done in future research is to analyze the surrounding area with LiDAR to see what effect it could have had on the landslide. And also, to see if there are hints of ancient landslides nearby that can help understand why the Stenungsund landslide happened and how it behaved.

5 Conclusion

The spatial change of the surface is that a large amount of landmass (≈ 90 000 m^3) has been displaced and transported from the upper part of the slope to the lower part and passed the slope. It did not move completely uniformly and had two directions (northwest and north) based on the vector displacement. The landslide has left behind a significant large scar (> 100 000 m^2) which is bottle-shaped near the main scarp and spreads lateral further down the slope towards northwest. The surface in the scar is more irregular and uneven compared to the surface from before the landslide.

Morphological features that were detected is ridges, scarps, ponds and cracks that were in specific areas depending on the type of feature: The cracks were located along buildings and infrastructure and explained how the landslide has dislocated the highway and pressed against the buildings. The scarps that were identified is the boundary for the landslides scar and simplified the analysis of the scar shape. The ridges were mainly in the upper part and nearby the main scar. These were perpendicular to the landslide and explained where the landslide was first initiated. The ponds were located between the ridges and cracks and did not add much to understand the movement of the landslide, but it showed how uneven and irregular the surface is.

Based on the change analysis, The landslide is interpreted to be a translational progressive landslide with a depletion zone and an accumulation zone. Thus, the movement has probably started in the upper part of the landslide. There are signs of retrogressive behavior based on the ridges, and by linking the ridges to the heaving zones there might have been two major flows during the landslide event.

As a final conclusion, this study has proved that LiDAR is an important and useful tool for landslide investigation. Through the analysis, I have been able to understand and interpret how the landslide has moved and the extent of it. The minor field observation was yet valuable and if more time had been devoted to this in the thesis, even more information could have been obtained. Thus, future survey's have great opportunity to experiment with LiDAR together with field observation, to be able to understand how landslides have occurred, but also to prevent future landslides in this region.

Acknowledgement

First of all, I would like to thank my supervisor Heather Reese who proposed to investigate the Stenungsund landslide and has supported and helped me throughout this project. Thanks also to my assistant supervisor Christian Öhrling at the Swedish Geological Survey and the compony Swedron who have contributed with data and valuable knowledge about the study area. Finaly, I would also like to thank my fellow students for the support and motivation we have given each other.

7 References

Andersson-Sköld, Y., Torrance, J. K., Lind, B., Odén, K., Stevens, R. L., & Rankka, K. (2005). Quick clay—A case study of chemical perspective in Southwest Sweden. *Engineering Geology*, *82*(2), 107-118. https://doi.org/https://doi.org/10.1016/j.enggeo.2005.09.014

Bäckström, K., & Linder, A. (2021). Fault Tree Analysis of Quick Clay Slides. In.

Barbarella, M., Fiani, M., & Lugli, A. (2014). APPLICATION OF LIDAR-DERIVED DEM FOR DETECTION OF MASS MOVEMENTS ON A LANDSLIDE. *Int. Arch. Photogramm. Remote Sens. Spatial Inf. Sci.*, *XL-5/W3*, 89-98. https://doi.org/10.5194/isprsarchives-XL-5-W3-89-2013

Bossi, G., Cavalli, M., Crema, S., Frigerio, S., Quan Luna, B., Mantovani, M., Marcato, G., Schenato, L., & Pasuto, A. (2015a). Multi-temporal LiDAR-DTMs as a tool for modelling a complex landslide: a case study in the Rotolon catchment (eastern Italian Alps). *Nat. Hazards Earth Syst. Sci.*, *15*(4), 715-722. https://doi.org/10.5194/nhess-15-715-2015

Bossi, G., Cavalli, M., Crema, S., Frigerio, S., Quan Luna, B., Mantovani, M., Marcato, G., Schenato, L., & Pasuto, A. (2015b). Multi-temporal LiDAR-DTMs as a tool for modelling a complex landslide: A case study in the Rotolon catchment (eastern Italian Alps). *Natural Hazards and Earth System Sciences*, *15*(4), 715-722. https://doi.org/10.5194/nhess-15-715-2015

Byggindustrin. (2023). *Raset i Stenungsund: Kan kosta "upp till någon miljard" att återställa.* https://www.byggindustrin.se/affarer-och-samhalle/hallbarhet/raset-i-stenungsund-kan-kosta-upp-till-nagon-miljard-att-aterstalla/

Campbell, J. B. (2022). *Introduction to Remote Sensing* (6th edition. ed.). New York : Guilford Publications.

Chen, Z., Gao, B., & Devereux, B. (2017). State-of-the-Art: DTM Generation Using Airborne LIDAR Data. *Sensors*, *17*(1), 150. https://www.mdpi.com/1424-8220/17/1/150

Chen, Z., Zhang, B., Han, Y., Zuo, Z., & Zhang, X. (2014). Modeling Accumulated Volume of Landslides Using Remote Sensing and DTM Data. *Remote Sensing*, *6*(2), 1514-1537. https://www.mdpi.com/2072-4292/6/2/1514

CloudCompare. (2020). *3D point cloud and mesh processing software Open Source Project.* https://www.danielgm.net/cc/

Dagens Samhälle. (n.d). *Begär 270 miljoner av regeringen efter E6-skredet- "vi behöver hjälp"*. Retrieved 2024-04-01 from: https://www.dagenssamhalle.se/offentlig-ekonomi/kommunal-ekonomi/begar-270-miljoner-av-regeringen-efter-e6-skredet-vi-behover-hjalp/

DJI Terra. (n.d). *Downloads*. Retrieved 2024-03-29 from: https://enterprise.dji.com/dji-terra

Eker, R., Aydın, A., & Hübl, J. (2017). Unmanned aerial vehicle (UAV)-based monitoring of a landslide: Gallenzerkogel landslide (Ybbs-Lower Austria) case study. *Environmental Monitoring and Assessment*, *190*(1), 28. https://doi.org/10.1007/s10661-017-6402-8

Fernández, T., Pérez, J. L., Cardenal, J., Gómez, J. M., Colomo, C., & Delgado, J. (2016). Analysis of Landslide Evolution Affecting Olive Groves Using UAV and Photogrammetric Techniques. *Remote Sensing*, *8*(10), 837. https://www.mdpi.com/2072-4292/8/10/837

Fredén, C. (1987). *Beskrivning till jordartskartan Marstrand NO/Göteborg NV*. Sveriges geologiska undersökning.

Geodose. (2020). *How to Calculate Raster Surface Volume in QGIS.* https://www.geodose.com/2020/07/how-to-calculate-raster-surface-volume-qgis.html

Hartlén, J. (1984). *Tuveskredet. Slutrapport*. Statens geotekniska institut.

Hekules. (n.d). Retrieved 2024-04-05 from: https://herkules.slu.se/get/

Hungr, O., Leroueil, S., & Picarelli, L. (2014). The Varnes classification of landslide types, an update. *Landslides*, *11*(2), 167-194. https://doi.org/10.1007/s10346-013-0436-y

Jaboyedoff, M., Oppikofer, T., Abellán, A., Derron, M.-H., Loye, A., Metzger, R., & Pedrazzini, A. (2012). Use of LIDAR in landslide investigations: a review. *Natural Hazards*, *61*(1), 5-28. https://doi.org/10.1007/s11069-010-9634-2

Johansson, M. (2009). Analys av samhällsekonomisk kostnad. Skredet vid E6 i småröd, 2006. In.

Joon-Kyu, P., Joong-Hyeok, H., & Keun-Wang, L. (2024). Applicability Analysis of Drone LiDAR through Comparison with Manned Airborne LiDAR. *Journal of Coastal Research*, *116*(sp1), 210-210. https://doi.org/10.2112/JCR-SI116-043.1

Kartvisaren. (n.d). Retrieved 2024-04-27 from: https://apps.sgu.se/kartvisare/

L'Heureux, J.-S. (2013). Characterisation of historical quick clay landslides and input parameters for Q-Bing.

L'heureux, J. (2012). A study of the retrogressive behaviour and mobility of Norwegian quick clay landslides. *Landslide and engineered slopes: protecting society through improved understanding. Taylor & Francis Group, London*, 981-988.

Lato, M., Porter, M., Hensold, G., McDougall, S., Kromer, R., & Gaib, S. (2016). Understanding landslide movement and kinematics with airborne lidar. Proceedings of 69th Canadian Geotechnical Society Conference, GeoVancouver,

Lato, M. J., Diederichs, M. S., & Hutchinson, D. J. (2010). Bias Correction for View-limited Lidar Scanning of Rock Outcrops for Structural Characterization. *Rock Mechanics and Rock Engineering*, *43*(5), 615-628. https://doi.org/10.1007/s00603-010-0086-5

Liu, Z., Qiu, H., Ma, S., Yang, D., Pei, Y., Du, C., Sun, H., Hu, S., & Zhu, Y. (2021). Surface displacement and topographic change analysis of the Changhe landslide on September 14, 2019, China. *Landslides*, *18*(4), 1471-1483. https://doi.org/10.1007/s10346-021-01626-4

Locat, A., Leroueil, S., Bernander, S., Demers, D., Jostad, H. P., & Ouehb, L. (2011). Progressive failures in eastern Canadian and Scandinavian sensitive clays. *Canadian Geotechnical Journal*, *48*(11), 1696-1712. https://doi.org/10.1139/t11-059

Mora, O. E., Lenzano, M. G., Toth, C. K., Grejner-Brzezinska, D. A., & Fayne, J. V. (2018). Landslide Change Detection Based on Multi-Temporal Airborne LiDAR-Derived DEMs. *Geosciences*, *8*(1), 23. https://www.mdpi.com/2076-3263/8/1/23

Okyay, U., Telling, J., Glennie, C. L., & Dietrich, W. E. (2019). Airborne lidar change detection: An overview of Earth sciences applications. *Earth-Science Reviews*, *198*, 102929.

Pellicani, R., Argentiero, I., Manzari, P., Spilotro, G., Marzo, C., Ermini, R., & Apollonio, C. (2019). UAV and Airborne LiDAR Data for Interpreting Kinematic Evolution of Landslide Movements: The Case Study of the Montescaglioso Landslide (Southern Italy). *Geosciences*, *9*(6).

QGIS.D. (n.d). *Raster Calculator*.

QGIS. (2024). *Download QGIS for your platform*. https://qgis.org/en/site/forusers/download.html

QGIS Documentation. (n.d). *Raster Calculator*. Retrieved 2024-04-06 from: https://docs.qgis.org/2.18/en/docs/user_manual/working_with_raster/raster_calculator.html

QGIS Documentation. (n.d.b). *Zonal Statistics Plugin.* Retrieved 2024-04-06 from: https://docs.qgis.org/2.18/en/docs/user_manual/plugins/plugins_zonal_statistics.html

QGIS Documentation. (n.d.c). *8.1. Lesson: Raster to Vector Conversion.* Retrieved 2024-04-09from:https://docs.qgis.org/3.34/en/docs/training_manual/complete_analysis/raster_to_vector.html

QGIS Plugins. (n.d). *LAStools.* Retrieved 2024-04-15 from: https://plugins.qgis.org/plugins/LAStools/

QGIS Plugins. (n.d.b). *Profile tool.* Retrieved 2024-04-15 from: https://plugins.qgis.org/plugins/LAStools/

QGIS Plugins. (n.d.c). *Points2One*. Retrieved 2024-04-14 from: https://plugins.qgis.org/plugins/points2one/

Rankka, K., Andersson-Sköld, Y., Hultén, C., Larsson, R., Leroux, V., & Dahlin, T. (2004). Quick clay in Sweden. In: Statens geotekniska institut.

Razak, K. A., Santangelo, M., Van Westen, C. J., Straatsma, M. W., & de Jong, S. M. (2013). Generating an optimal DTM from airborne laser scanning data for landslide mapping in a tropical forest environment. *Geomorphology*, *190*, 112-125.

Salas-Romero, S., Malehmir, A., Snowball, I., Lougheed, B. C., & Hellqvist, M. (2016). Identifying landslide preconditions in Swedish quick clays—insights from integration of surface geophysical, core sample- and downhole property measurements. *Landslides*, *13*(5), 905-923. https://doi.org/10.1007/s10346-015-0633-y

Shih, K.-T., Balachandran, A., Nagarajan, K., Holland, B., Slatton, K., & George, A. (2008). *Fast real-time LIDAR processing on FPGAs*.

Svenskt Vatten. (2024). *Skredet på E6 – från räddningsinsats till strategiskt systemtänk.* https://www.svensktvatten.se/om-oss/nyheter-lista/skredet-pa-e6--fran-raddningsinsats-till-strategiskt-systemtank/

Sveriges Radio. (2023). *Schaktmassorna som förstörde E6 – en mångmiljonaffär.* https://sverigesradio.se/artikel/landslide-devastates-crucial-motorway-in-western-sweden

SVT Nyheter. (n.d). *Skredet vid E6 i Stenungsund.* Retrieved 2024-03-29 from: https://www.svt.se/nyheter/om/vagraset-pa-e6-i-stenungsund

Telbisz, T., Látos, T., Deák, M., Székely, B., Koma, Z., & Standovár, T. (2016). The advantage of lidar digital terrain models in doline morphometry compared to topographic map based datasets–Aggtelek karst (Hungary) as an example. *Acta Carsologica*, *45*(1).

Torrance, J. K. (2012). Landslides in quick clay. *Landslides: types, mechanisms and modeling. Cambridge University Press, Cambridge*, 83-94.

Tseng, C. M., Lin, C. W., Stark, C. P., Liu, J. K., Fei, L.-Y., & Hsieh, Y.-C. (2013). Application of a multi-temporal, LiDAR-derived, digital terrain model in a landslide-volume estimation. *Earth Surface Processes and Landforms*, *38*.

With, C., Löfroth, H., Bastani, M., Persson, L., Rodhe, L., Hedfors, J., & Schoning, K. (2022). A methodology for mapping of quick clay in Sweden. *Natural Hazards*, *112*(3), 2549-2576. https://doi.org/10.1007/s11069-022-05278-y

Yunfei, B., Guoping, L., Chunxiang, C., Xiaowen, L., Hao, Z., Qisheng, H., Linyan, B., & Chaoyi, C. (2008). Classification of LIDAR point cloud and generation of DTM from LIDAR height and intensity data in forested area. *The International Archives of the Photogrammetry, Remote Sensing and Spatial Information Sciences*, *37*(7), 313-318.

Zhuo, X., Koch, T., Kurz, F., Fraundorfer, F., & Reinartz, P. (2017). Automatic UAV Image Geo-Registration by Matching UAV Images to Georeferenced Image Data. *Remote Sensing*, *9*. https://doi.org/10.3390/rs9040376

8 Appendix

A)

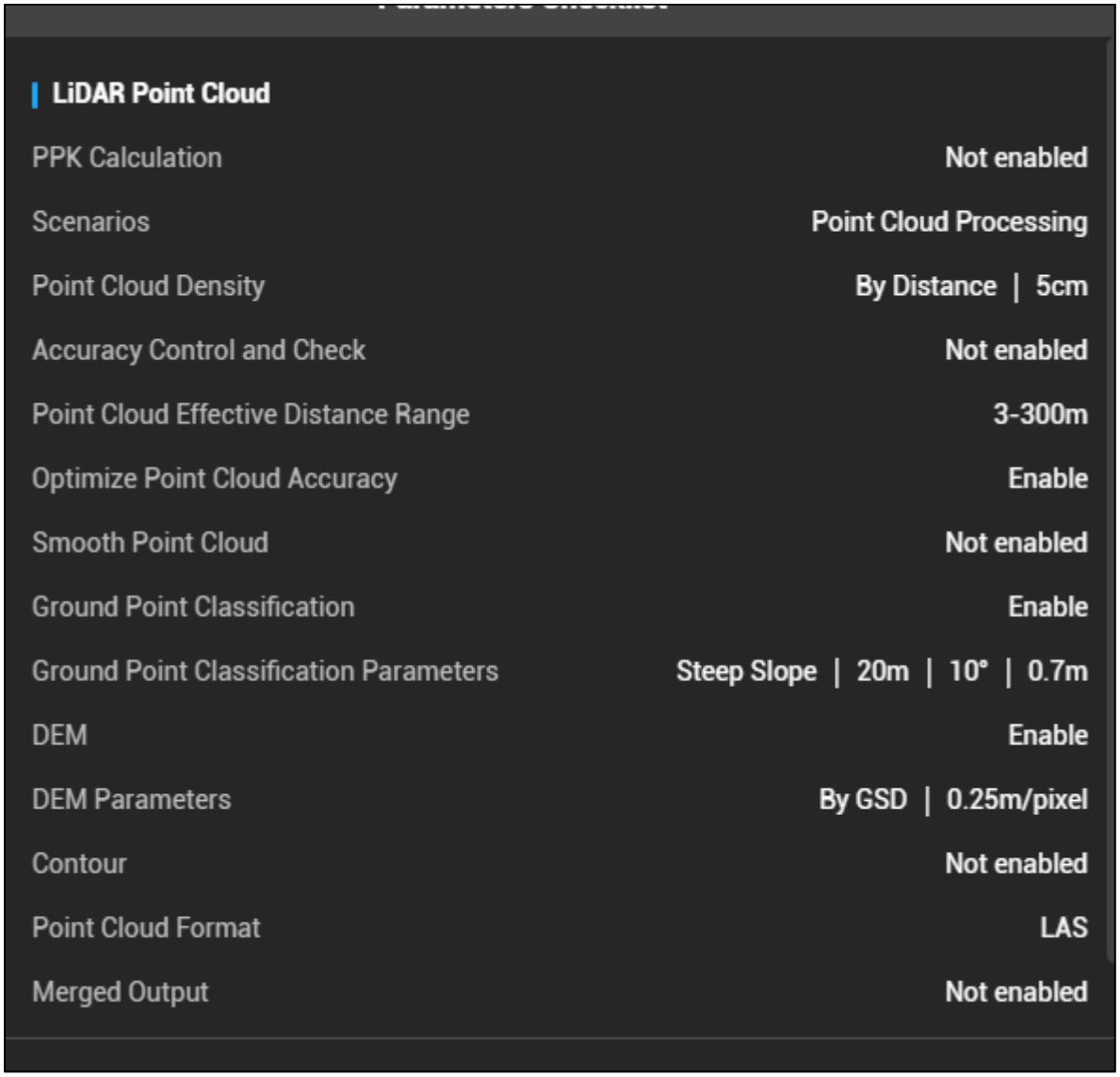

LiDAR Point Cloud	
PPK Calculation	Not enabled
Scenarios	Point Cloud Processing
Point Cloud Density	By Distance | 5cm
Accuracy Control and Check	Not enabled
Point Cloud Effective Distance Range	3-300m
Optimize Point Cloud Accuracy	Enable
Smooth Point Cloud	Not enabled
Ground Point Classification	Enable
Ground Point Classification Parameters	Steep Slope | 20m | 10° | 0.7m
DEM	Enable
DEM Parameters	By GSD | 0.25m/pixel
Contour	Not enabled
Point Cloud Format	LAS
Merged Output	Not enabled

B)

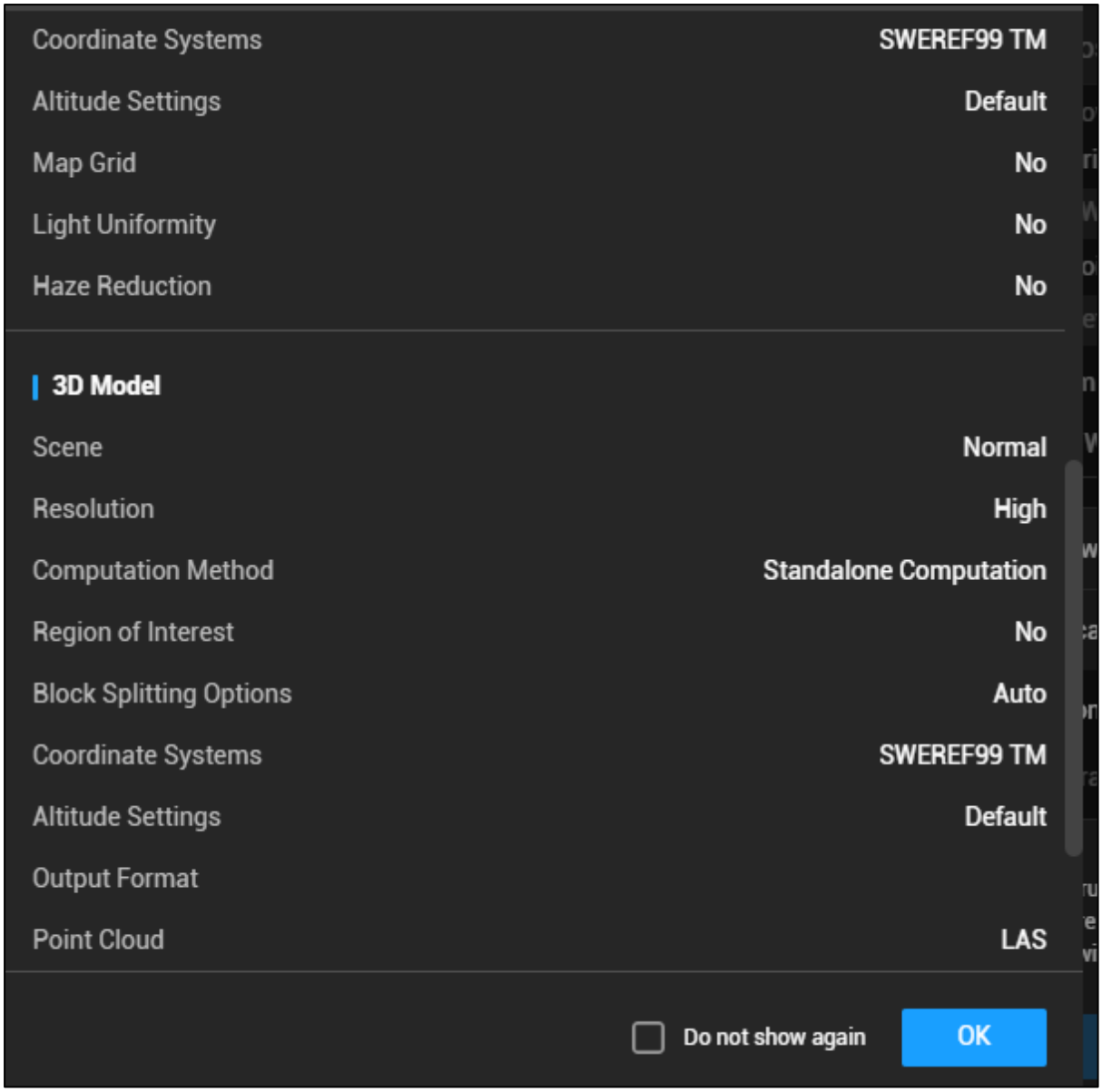
Coordinate Systems
SWEREF99 TM
Altitude Settings
Default
Map Grid
No
Light Uniformity
No
Haze Reduction
No
3D Model
Scene
Normal
Resolution
High
Computation Method
Standalone Computation
Region of Interest
No
Block Splitting Options
Auto
Coordinate Systems
SWEREF99 TM
Altitude Settings
Default
Output Format
Point Cloud
LAS
Do not show again
OK